Electronic Supplementary Material (ESI) for RSC Advances

Anion Templated Assembly of [2]Catenanes Selective for Chloride in Aqueous Solvent Media

Supplementary Information

Nicholas H. Evans, Emma S. H. Allinson, Michael D. Lankshear, Ka-Yuen Ng, Andrew R. Cowley, Christopher J. Serpell, Sérgio M. Santos, Paulo J. Costa, Vítor Félix, and Paul D. Beer*

Inorganic Chemistry Laboratory, Department of Chemistry, University of Oxford, South Parks Road, Oxford. OX1 3QR (UK).

Departmento de Química, CICECO and Secção Autónoma de Ciências da Saûde, Universidade de Aveiro, 3810-193, Aveiro (Portugal).

Electronic Supplementary Material (ESI) for RSC Advances

Anion Templated Assembly of [2]Catenanes Selective for Chloride in Aqueous Solvent Media

Supplementary Information

Table of Contents

Experimental Section

General Notes

NMR spectra were recorded on Varian Mercury 300 and Unity Plus 500, and Bruker AVII 500 (with ^{13}C Cryoprobe) spectrometers. Mass spectrometry was carried out on a Micromass LCT Premier XE spectrometer and accurate masses were obtained to 4 decimal places using Bruker microTOF and Micromass GCT spectrometers. Melting points were recorded on a Gallenkamp capillary melting point apparatus and are uncorrected. Elemental analyses were performed by the service at the Inorganic Chemistry Laboratory, University of Oxford.

All commercially available solvents and chemicals were used as obtained, without further purification, unless otherwise stated. Triethylamine was dried and stored over potassium hydroxide. $(TBA)_2SO_4$ was prepared by concentrating a commercially available aqueous solution, then azeotroping the residue with dry THF with the resulting solid being dried and stored over P_2O_5 in a desiccator. Grubbs' 1st and 2nd Generation Catalysts, $AgPF_6$ and tetrabutylammonium (TBA) salts were stored prior to use in a desiccator, under vacuum, that contained P_2O_5 and self-indicating silica. Deionised water was used in all cases. When stated as dry, solvents were prepared by degassing with N_2 then drying by passing through an MBraun MPSP-800 column and used immediately.

3, 5-bis-chloro-carbonyl pyridine and 5-*tert*-butylisophthaloyl dichloride were prepared by refluxing the appropriate commercially available diacid in excess $SOCl_2$ under an atmosphere of N_2 until no solid remained. The reaction mixture was allowed to cool to room temperature and excess $SOCl_2$ was removed *in vacuo*. The product was immediately used, with the reaction assumed to have occurred in quantitative yield.

Synthetic Procedures & Characterization

The preparation and characterization of compounds $\mathbf{1}^+(X^-)$,[1] $\mathbf{2}^+(X^-)$,[2] **4**,[1] **5**,[2, 3] **7**,[1] **8**,[2] $\mathbf{10}^{2+}(X^-)(Y^-)$[1] and $\mathbf{15}^+(Cl^-)$[4] where X^-, Y^- = Cl^- or PF_6^- (and I^-, for $\mathbf{1}^+$ and $\mathbf{2}^+$) have all been reported previously.

Synthesis and characterization of catenanes $\mathbf{11}^{2+}(X^-)(Y^-)$:

Procedure
[2]Catenanes $\mathbf{11}^{2+}(X^-)(Y^-)$ were prepared by stirring one equivalent of precursor $\mathbf{X}^+(X^-)$ (0.038 mmol) and one equivalent of precursor $\mathbf{X}^+(Y^-)$ (0.038 mmol) in dry CH_2Cl_2 (25 mL) for 20 minutes. Grubbs' catalyst (10% by wt) was then added, and the reaction mixture was stirred under an atmosphere of N_2 for 16 h. Purification by silica gel preparatory TLC (CH_2Cl_2/CH_3OH 92:8 or CH_2Cl_2/CH_3OH 88:12), gave the [2]catenanes as yellow films with yields as stated in Table 1 of the main article.

[2]Catenane $\mathbf{11}^{2+}(PF_6^-)_2$ was also prepared by washing a solution of $\mathbf{11}^{2+}(Cl^-)_2$ (13 mg, 0.010 mmol) dissolved in $CHCl_3$ (10 mL) with 0.1 M NH_4PF_6 (15 × 2 mL), then H_2O

(10 × 10 mL). The organic layer was then separated, dried over $MgSO_4$ and solvent removed *in vacuo* to give the product as a yellow solid (15 mg, quant.).

Characterization

[2]Catenane 11^{2+}(Cl^-)$_2$

Mt. pt. = 146°C (dec.); δ_H(300 MHz; CD_3CN): 9.54 (2H, s, *para*-pyridinium Ar*H*), 9.14 (4H, s, *ortho*-pyridinium Ar*H*), 8.79 (4H, t, ^3J = 3.7 Hz, N*H*), 6.57 (8H, d, ^3J = 8.9 Hz, hydroquinone Ar*H*) 6.31 (8H, d, ^3J = 8.9 Hz, hydroquinone Ar*H*), 6.04 (4H, dt, ^3J = 2.7 Hz, ^3J = 1.4 Hz, CH_2CH=CH), 4.44 (6H, s, N^+CH_3), 4.05–4.11 (16H, m, CH_2CH=CH & OCH_2), 3.78–3.81 (8H, m, OCH_2), 3.64–3.74 (16H, m, OCH_2 & NHCH_2); δ_C(75.5 MHz; CD_3CN): 161.5, 153.8, 153.4, 147.5, 140.2, 133.6, 130.8, 115.8, 115.4, 71.5, 70.0, 68.9, 66.4, 42.0 (one aliphatic *C* missing); m/z (ES): 592.2643 ([M − 2Cl]$^{2+}$, $C_{64}H_{76}N_6O_{16}$ requires 592.2653).

[2]Catenane 11^{2+}(Cl^-)(PF_6^-)

Mt. pt. = 126-134°C; δ_H(300 MHz; CD_3CN): 9.17 (2H, br. s, *para*-pyridinium Ar*H*), 8.85 (4H, br. s, *ortho*-pyridinium Ar*H*), 7.98 (4H, br. s, N*H*), 6.56 (8H, d, ^3J = 8.6 Hz, hydroquinone Ar*H*), 6.36 (8H, d, ^3J = 8.6 Hz, hydroquinone Ar*H*), 6.04 (4H, t, ^3J = 2.8 Hz, C*H*=C*H*), 4.45 (6H, s, N^+CH_3), 4.04–4.10 (16H, m, CH_2CH=CH & OCH_2), 3.86 (8H, br. s, OCH_2), 3.68–3.75 (16H, m, OCH_2 & NHCH_2); δ_C(75.5 MHz; CD_3CN): 161.5, 153.7, 153.5, 146.8, 140.8, 134.1, 131.0, 115.9, 115.7, 71.5, 70.0, 69.1, 66.9, 50.5, 41.2; δ_F(282.4 MHz; CD_3CN): −72.8 (d, ^1J = 707 Hz, PF_6^-); m/z (ES): 592.2652 ([M]$^{2+}$, $C_{64}H_{76}N_6O_{16}$ requires 592.2653).

[2]Catenane 11^{2+}(PF_6^-)$_2$

Mt. pt. = 126°C; δ_H(300 MHz; CD_3CN): 9.07 (2H, s, *para*-pyridinium Ar*H*), 8.76 (4H, s, *ortho*-pyridinium Ar*H*), 7.85 (4H, br. s, N*H*), 6.55 (8H, d, ^3J = 8.2 Hz, hydroquinone Ar*H*), 6.40 (8H, d, ^3J = 8.2 Hz, hydroquinone Ar*H*), 6.03 (4H, app. s, C*H*=C*H*), 4.45 (6H, s, N^+CH_3), 4.03–4.09 (16H, m, CH_2CH=CH & OCH_2), 3.90 (8H, br. s, OCH_2), 3.71–3.76 (16H, m, OCH_2 & NHCH_2); δ_C(125.8 MHz; CD_3CN): 161.5, 153.7, 153.6, 146.5, 141.2, 134.4, 131.0, 115.9, 115.8, 71.5, 70.0, 69.2, 67.1, 50.7, 41.0; δ_F(282.4 MHz; CD_3CN): -72.9 (d, ^{1}J = 706 Hz, PF_6^-); δ_F(282.4 MHz; CD_3CN): -72.9 (d, ^{1}J = 706 Hz, PF_6^-); m/z (ES): 592.2649 ([M]$^{2+}$, $C_{64}H_{76}N_6O_{16}$ requires 592.2653); Elemental analysis found: C 51.1; H 5.3; N 5.4. $C_{64}H_{76}N_6O_{16}(PF_6)_2$•0.5($CH_2Cl_2$) requires C 51.0; H 5.1; N 5.5.

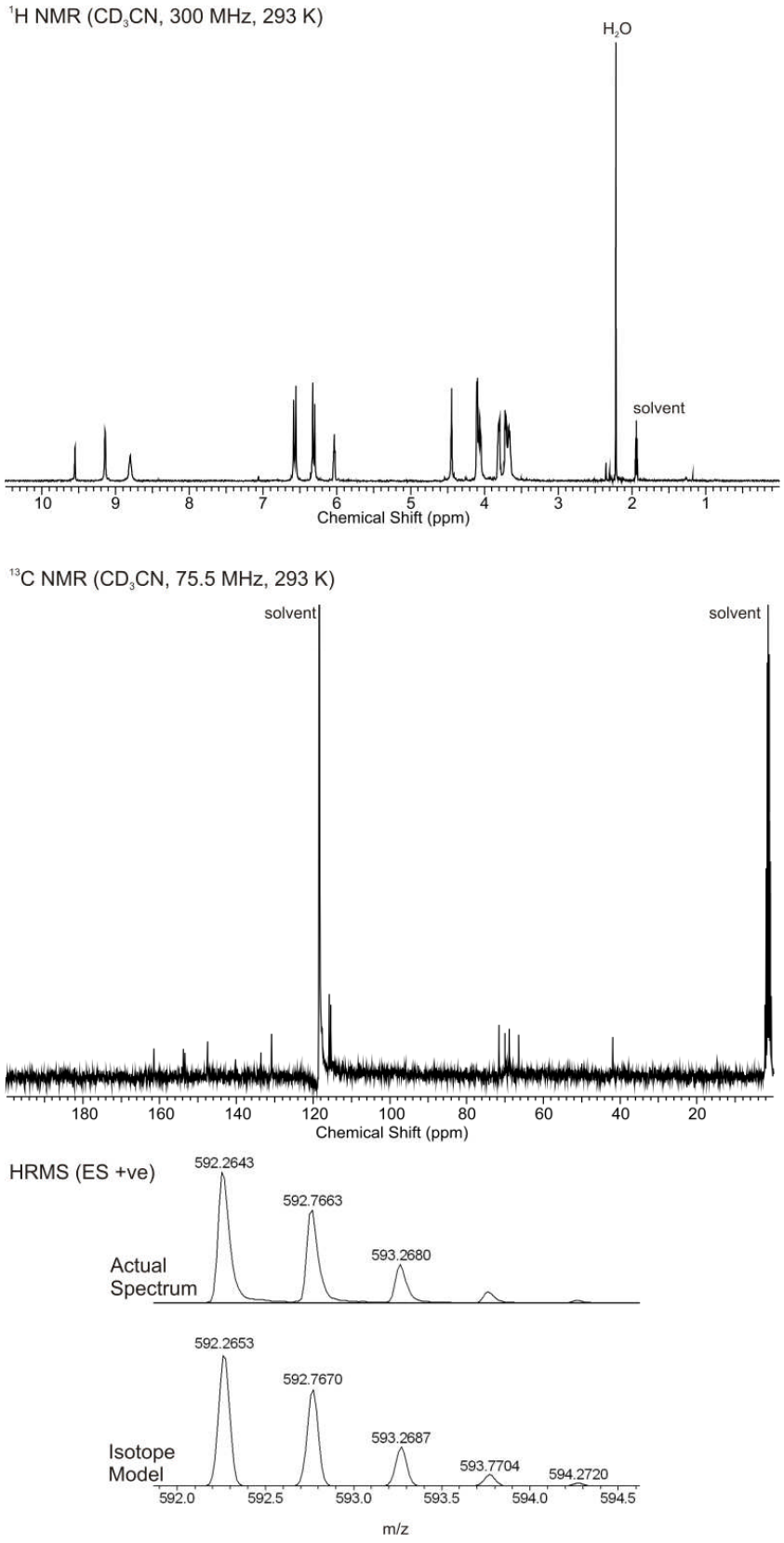

Figure S1: Spectral characterization of [2]catenane $\mathbf{11}^{2+}(Cl^-)_2$.

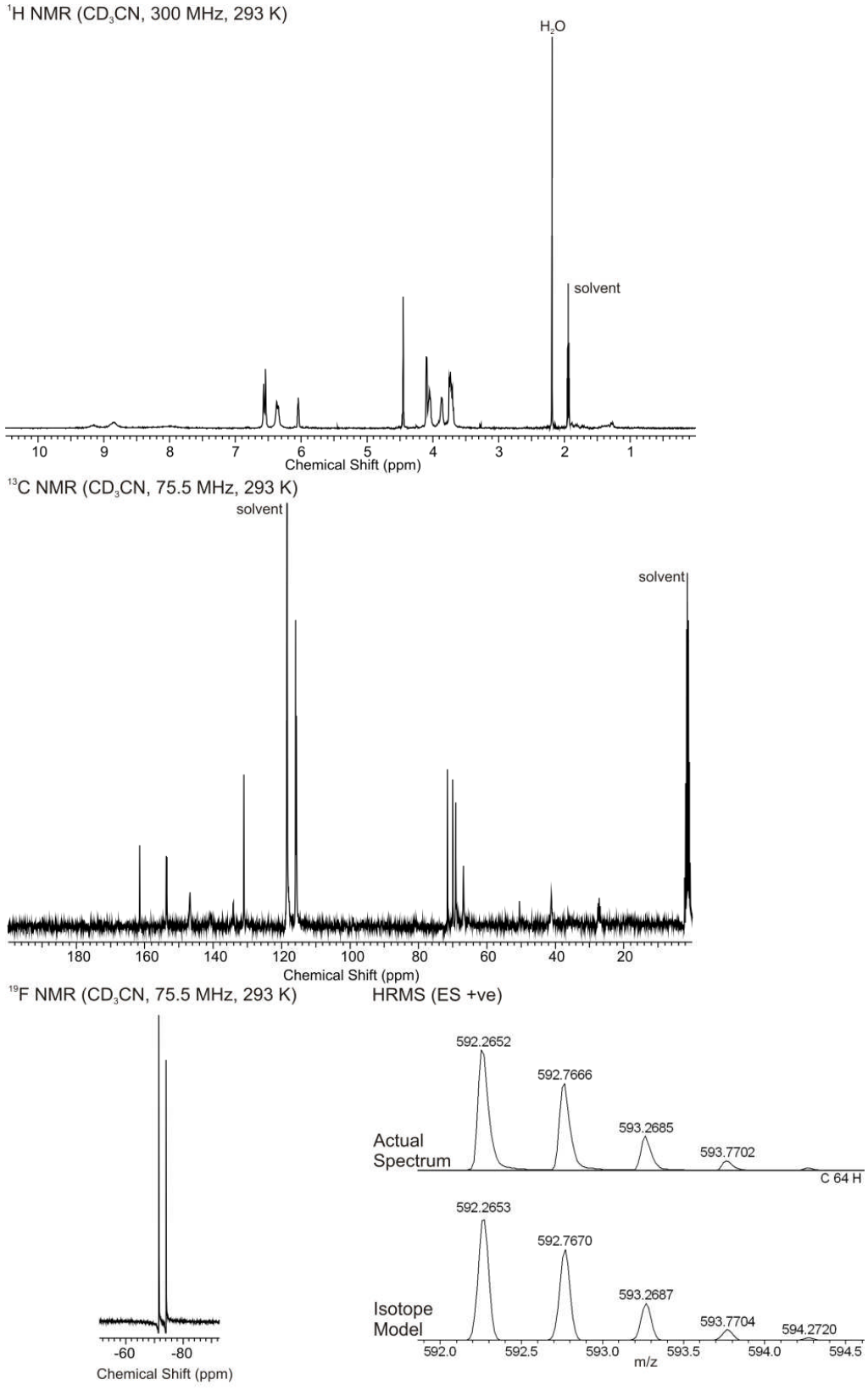

Figure S2: Spectral characterization of [2]catenane $\mathbf{11}^{2+}(Cl^-)(PF_6^-)$.

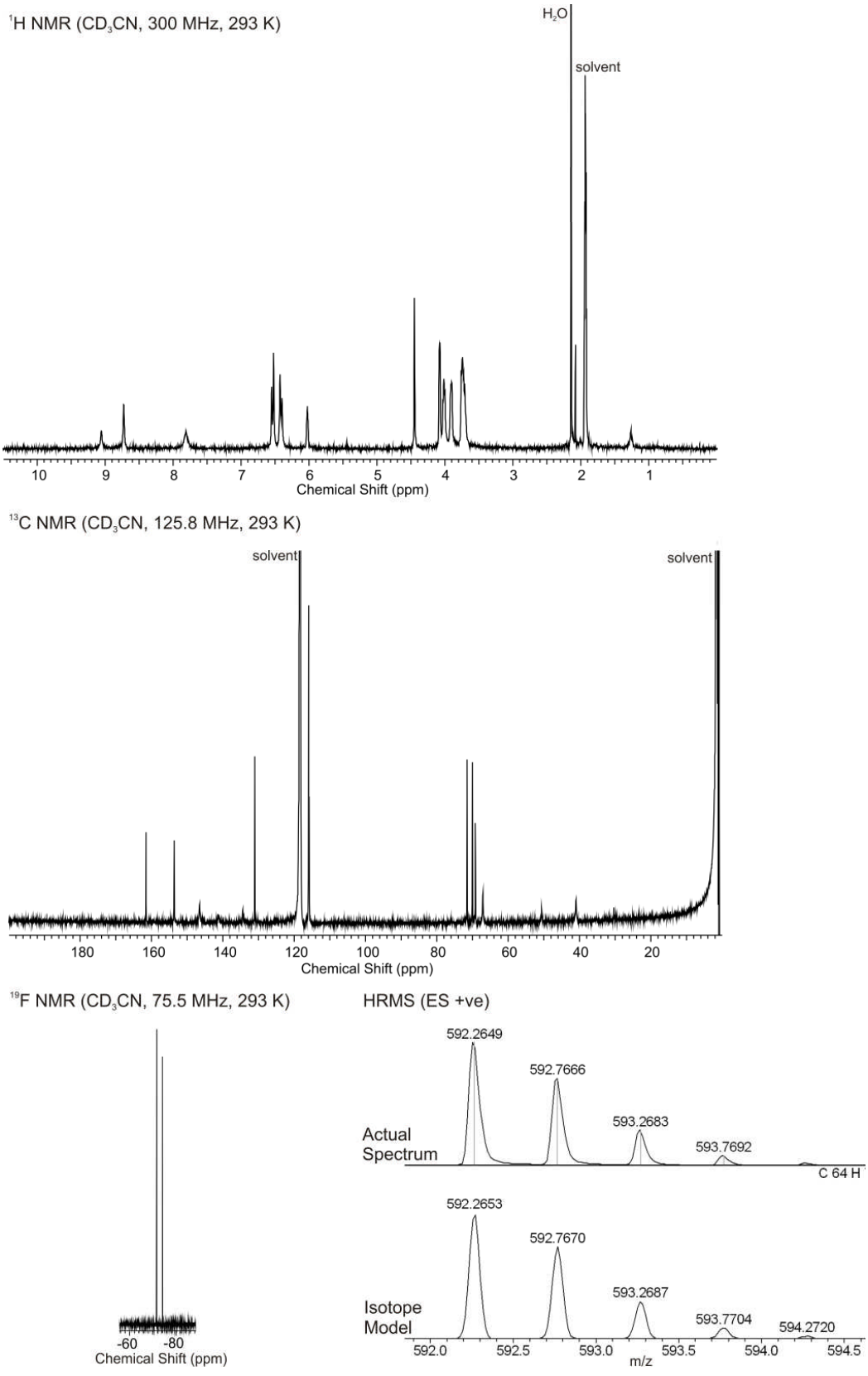

Figure S3: Spectral characterization of [2]catenane $\mathbf{11}^{2+}(PF_6^-)_2$.

Synthesis of compounds **6**, **7**, **3**$^{+}$(X^{-}) X^{-} = I^{-}, Cl^{-}, PF_6^{-}, **13**$^{+}$(Cl^{-}), **14** & **15**

2-(4-(Allyloxy)phenoxy)acetonitrile **(S-1)** was prepared by literature procedures.[5]

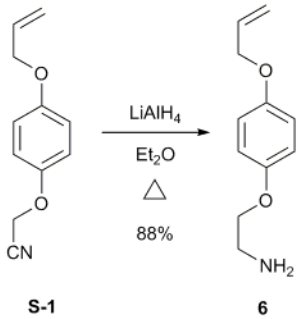

Scheme S1: Synthesis of compound **6**.

Compound **6**

A solution of 2-(4-(allyloxy)phenoxy)acetonitrile **S-1**[5] (1.20 g, 6.31 mmol) in dry Et_2O (30 mL) was slowly added to a suspension of $LiAlH_4$ (0.36 g, 9.47 mmol) in dry Et_2O (20 mL) and the mixture was then heated under reflux for 1 h under a N_2 atmosphere. The reaction was allowed to cool to RT and H_2O (0.36 mL) was added dropwise (CAUTION! — highly exothermic) followed by 15% $NaOH_{(aq)}$ (0.36 mL) and then further H_2O (1.08 mL). The white precipitate was then filtered and washed with Et_2O (100 mL). All organics were combined, dried over $MgSO_4$ and the solvent removed *in vacuo* to give a golden oil which on standing solidified into a white waxy solid (1.07 g, 88%). δ_H(300 MHz; $CDCl_3$): 6.85 (4H, s, Ar*H*), 6.01–6.10 (1H, m, C*H*=CH_2), 5.26–5.44 (2H, m, CH=C*H*$_2$), 4.49 (2H, dt, ^3J = 5.3 Hz, ^4J = 1.3 Hz, C*H*$_2$CH=CH_2), 3.94 (2H, t, ^3J = 5.1 Hz, C*H*$_2$$CH_2NH_2$), 3.06 (2H, t, ^3J = 5.1 Hz, CH_2C*H*$_2$$NH_2$), 1.48 (2H, br. s, N*H*$_2$); δ_C(75.5 MHz; $CDCl_3$): 153.1, 152.8, 133.5, 117.4, 115.6, 115.3, 70.7, 69.4, 41.6; m/z (FI): 193.1101 ($[M^{\bullet}]^+$, $C_{11}H_{15}NO_2$ requires 193.1103).

Compound **9**

Compound **6** (1.05 g, 5.43 mmol) was dissolved in dry CH_2Cl_2 (100 mL) with excess NEt_3 (4 mL) and the mixture cooled to 0°C. A solution of pyridine-3,5-biscarbonyl dichloride (0.55 g, 2.72 mmol) in dry CH_2Cl_2 (50 mL) was added dropwise to the reaction which was then stirred at RT for 1 h under a N_2 atmosphere. The product precipitated out during the course of the reaction and was filtered from the reaction mixture as a white solid (1.00 g, 71%). Mt. pt. = 188°C; δ_H(300 MHz; d_6-DMSO): 9.11 (2H, d, ^4J = 2.1 Hz, *ortho*-pyridyl Ar*H*), 9.05 (2H, t, ^3J = 5.4 Hz, N*H*CH_2), 8.63 (1H, t, ^4J = 2.1 Hz, *para*-pyridyl Ar*H*), 6.88 (8H, d, ^3J = 1.8 Hz, hydroquinone Ar*H*), 5.94–6.07 (2H, m, C*H*=CH_2), 5.20–5.39 (4H, m, CH=C*H*$_2$), 4.48 (4H, dt, ^3J = 5.1 Hz, ^4J = 1.7 Hz, C*H*$_2$CH=CH_2), 4.07 (4H, t, ^3J = 5.7 Hz, $NHCH_2$C*H*$_2$), 3.61–3.66 (4H, app. quartet, NHC*H*$_2$$CH_2$); δ_C(75.5 MHz; d_6-DMSO): 164.6, 152.5, 152.4, 150.5, 134.1, 134.0, 129.5, 117.2, 115.6, 115.4, 68.6, 66.4, 39.2; m/z (ES): 540.2101 ($[M + Na]^+$, $C_{29}H_{31}N_3NaO_6$ requires 540.2105).

Compound **3**$^{+}$(I^{-})

Compound **9** (1.00 g, 1.93 mmol) and MeI (5 mL) were dissolved in acetone (25 mL) and heated under reflux for 60 h. The reaction was then cooled to RT and the solvent was removed *in vacuo* to give the product as a bright yellow oily solid (1.25 g, 98%). δ_H(300 MHz; $CDCl_3$): 9.86 (1H, s, *para*-pyridinium Ar*H*), 9.35 (2H, s, *ortho*-pyridinium Ar*H*), 8.84 (2H, t, ^3J = 5.6 Hz, N*H*), 6.73–6.83 (8H, m, hydroquinone Ar*H*), 5.95–6.08 (2H, m, C*H*=CH_2), 5.24–5.42 (4H, m, CH=CH_2), 4.43–4.44 (7H, m, N^+CH_3 and $OCH_2CH=CH_2$), 4.16 (4H, t, ^3J = 5.4 Hz, $NHCH_2CH_2$), 3.79–3.85 (4H, app. quartet, $NHCH_2CH_2$); δ_C(75.5 MHz; $CDCl_3$): 160.7, 152.9, 152.5, 146.2, 141.4, 133.6, 133.3, 117.6, 115.8, 115.6, 69.4, 66.5, 49.4, 40.1; m/z (ES): 532.2457 ([M − I]$^+$, $C_{30}H_{34}N_3O_6$ requires 532.2442).

Compound **3**$^{+}$(Cl^{-})

A solution of **3**$^{+}$(I^{-}) (1.22 g, 1.85 mmol) in $CHCl_3$ (150 mL) was shaken vigorously in a separating funnel with 1M $NH_4Cl_{(aq)}$ (8 × 150 mL). The organic layer was then washed with H_2O (2 × 75 mL), dried over $MgSO_4$ and the solvent removed to give an oily yellow solid (0.90 g, 86%). Mt. pt. = 147°C; δ_H(300 MHz; $CDCl_3$): 10.43 (1H, s, *para*-pyridinium Ar*H*), 9.56 (2H, t, ^3J = 5.4 Hz, N*H*CH_2), 9.35 (2H, s, *ortho*-pyridinium Ar*H*), 6.74–6.87 (8H, m, hydroquinone Ar*H*), 5.96–6.09 (2H, m, C*H*=CH_2), 5.25–5.42 (4H, m, CH=CH_2), 4.44 (4H, dt, ^3J = 5.3 Hz, ^4J = 1.5 Hz, $OCH_2CH=CH_2$), 4.39 (3H, s, NCH_3), 4.16 (4H, t, ^3J = 5.6 Hz, $NHCH_2CH_2$), 3.78–3.83 (4H, app. quartet, $NHCH_2CH_2$); δ_C(75.5 MHz; $CDCl_3$): 160.4, 153.0, 152.7, 146.3, 141.7, 133.9, 133.4, 117.6, 115.9, 115.6, 69.4, 66.7, 49.2, 40.3; m/z (ES): 532.2428 ([M − Cl]$^+$, $C_{30}H_{34}N_3O_6$ requires 532.2442).

Compound **3**$^{+}$(PF_6^{-})

3^{+}(Cl^{-}) (150 mg, 0.26 mmol) was dissolved in dry CH_2Cl_2 (50 mL) in a round bottom flask protected from light. $AgPF_6$ (267 mg, 1.06 mmol) was then added, with the resulting mixture being stirred at RT in the absence of light under a N_2 atmosphere for 2 h. The solid residue was triturated with CH_3CN, filtered and the filtrate was concentrated *in vacuo* to give a yellow solid. This solid was then redissolved in CH_2Cl_2 (20 mL) and stirred with H_2O (20 mL) upon which the product precipitated out. The precipitate was collected by filtration and redissolved in CH_3CN. After removal of the solvent *in vacuo* the product was obtained as a yellow solid (170 mg, 95%). Mt. pt. = 148–152°C; δ_H(300 MHz; CD_3CN): 9.11 (2H, d, ^4J = 1.3 Hz, *ortho*-pyridinium Ar*H*), 9.03 (1H, t, ^4J = 1.3 Hz, *para*-pyridinium Ar*H*), 7.67–7.70 (2H, m, N*H*), 6.87 (8H, s, hydroquinone Ar*H*), 5.98–6.10 (2H, m, C*H*=CH_2), 5.21–5.41 (4H, m, CH=CH_2), 4.48 (4H, dt, ^3J = 5.1 Hz, ^4J = 1.7 Hz, $OCH_2CH=CH_2$), 4.38 (3H, s, N^+CH_3), 4.12 (4H, t, ^3J = 5.3 Hz, $NHCH_2CH_2$), 3.75–3.81 (4H, app. quartet, $NHCH_2CH_2$); δ_C(75.5 MHz; CD_3CN): 161.9, 154.0, 153.8, 147.7, 142.1, 135.3, 135.0, 117.7, 116.7, 116.6, 70.0, 67.5, 49.4, 41.0; δ_F(282.4 MHz; CD_3CN): −72.9 (d, ^1J = 709 Hz, PF_6^-); m/z (ES): 532.2438 ([M – PF_6]$^+$, $C_{30}H_{34}N_3O_6$ requires 532.2442).

Compound **13**$^{+}$(Cl^{-})

RCM precursor **3**$^{+}$Cl (20 mg, 0.035 mmol) was dissolved in dry CH_2Cl_2 (10 mL), and then Grubbs' 1st generation catalyst (2.0 mg, 10% by wt.) was added, with the resulting reaction mixture being stirred for 16 h under a constant flow of $N_{2(g)}$. During the course of the reaction, a yellow solid precipitated out. After solvent was removed *in vacuo* it was possible to identify the macrocyclic product in electrospray MS. However, the severe insolubility of the macrocyclic product prevented purification by either crystallisation or chromatographic methods. m/z (ES): 504.2127 ([M − Cl]$^{+}$, $C_{28}H_{30}N_3O_6$ requires 504.2129).

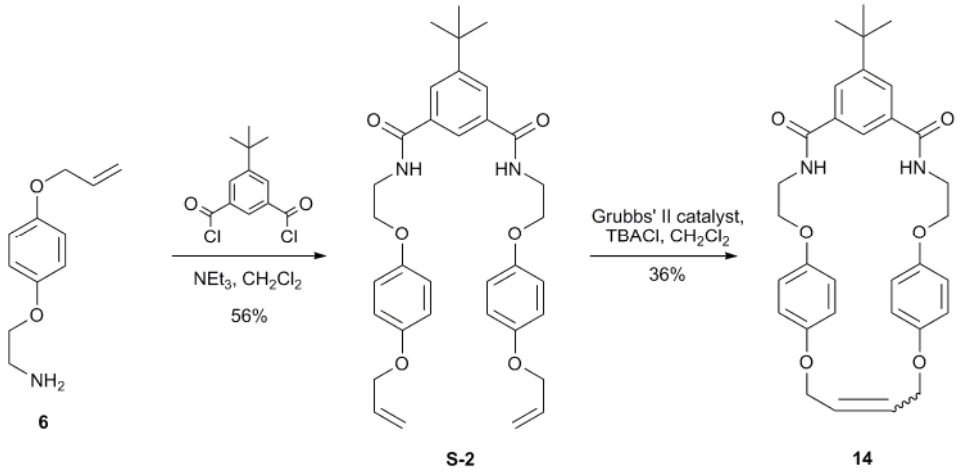

Scheme S2: Synthesis of macrocycle **14**.

Compound **S-2**. Compound **6** (0.87 g, 4.50 mmol) was dissolved in dry CH_2Cl_2 (100 mL) with excess NEt_3 (1.5 mL) and the mixture cooled to 0°C. A solution of 5-*tert*-butylisophthaloyl dichloride (0.58 g, 2.25 mmol) in dry CH_2Cl_2 (50 mL) was added dropwise to the reaction which was then stirred at RT for 16 h under a N_2 atmosphere. The reaction mixture was subsequently washed with 1 M HCl (3 × 100 mL) and brine (3 × 100 mL), dried over $MgSO_4$ and the solvent removed *in vacuo* to give the crude product which was purified using silica gel chromatography (CH_2Cl_2/CH_3OH 98.5:1.5) to give the product as a white solid (0.73 g, 56%). Mt. pt. = 88°C; δ_H(300 MHz; $CDCl_3$): 7.96 (2H, d, ^4J = 1.5 Hz, *ortho*-isophthalamide Ar*H*), 7.92–7.93 (1H, t, ^4J = 1.5 Hz, *para*-isophthalamide Ar*H*), 6.85 (8H, s, hydroquinone Ar*H*), 6.67 (2H, t, ^3J = 5.4 Hz, N*H*), 5.98–6.11 (2H, m, C*H*=CH_2), 5.25–5.44 (4H, m, CH=CH_2), 4.49 (4H, dt, ^3J = 5.3 Hz, ^4J = 1.6 Hz, OCH_2CH=CH_2), 4.12 (4H, t, ^3J = 5.0 Hz, NHCH_2CH_2), 3.84–3.89 (4H, app. quartet, NHCH_2CH_2), 1.36 (9H, s, CH(CH_3)$_3$); δ_C(75.5 MHz; $CDCl_3$): 167.3, 153.1, 152.6, 152.5, 134.5, 133.4, 127.4, 122.2, 117.5, 115.7, 115.4, 69.4, 67.2, 39.8, 35.0, 31.1; m/z (ES): 595.2774 ([M + Na]$^{+}$, $C_{34}H_{40}N_2NaO_6$ requires 595.2779).

Marcocycle **14**

Compound **S-2** (75 mg, 0.13 mmol) and TBACl (36 mg, 0.13 mmol) were dissolved in dry CH_2Cl_2 (50 mL) and stirred under a N_2 atmosphere for 20 min. Grubbs' 2nd generation catalyst (7.5 mg, 10% by wt) was then added and the reaction stirred at under a constant flow of $N_{2(g)}$ for 16 h. The solvent was removed *in vacuo* and the product purified using silica gel prep TLC (CH_2Cl_2/CH_3OH 98:2) to give the product as a white solid (27 mg, 36%). Mt. pt. = 238°C; δ_H(300 MHz; $CDCl_3$): 8.17 (2H, d, ^4J = 1.5 Hz, *ortho*-isophthalamide Ar*H*), 7.70 (1H, t, ^4J = 1.5 Hz, *para*-isophthalamide Ar*H*), 6.71–6.77 (10H, m, hydroquinone Ar*H* & N*H*), 5.85–5.86 (2H, m, C*H*=CH), 4.62 (4H, dd, ^3J = 2.4 Hz, ^4J = 1.2 Hz, OCH_2CH=CH), 4.08 (4H, t, ^3J = 4.9 Hz, NHCH$_2$CH_2), 3.85–3.90 (4H, app. quartet, NHCH_2), 1.37 (9H, s, CH(CH_3)$_3$); δ_C(75.5 MHz; $CDCl_3$): 167.1, 153.2, 152.8, 152.6, 134.3, 130.0, 128.7, 119.8, 117.1, 115.6, 68.8, 67.6, 39.4, 35.1, 31.1; m/z (ES): 567.2463 ([M + Na]$^+$, $C_{32}H_{36}N_2NaO_6$ requires 567.2466).

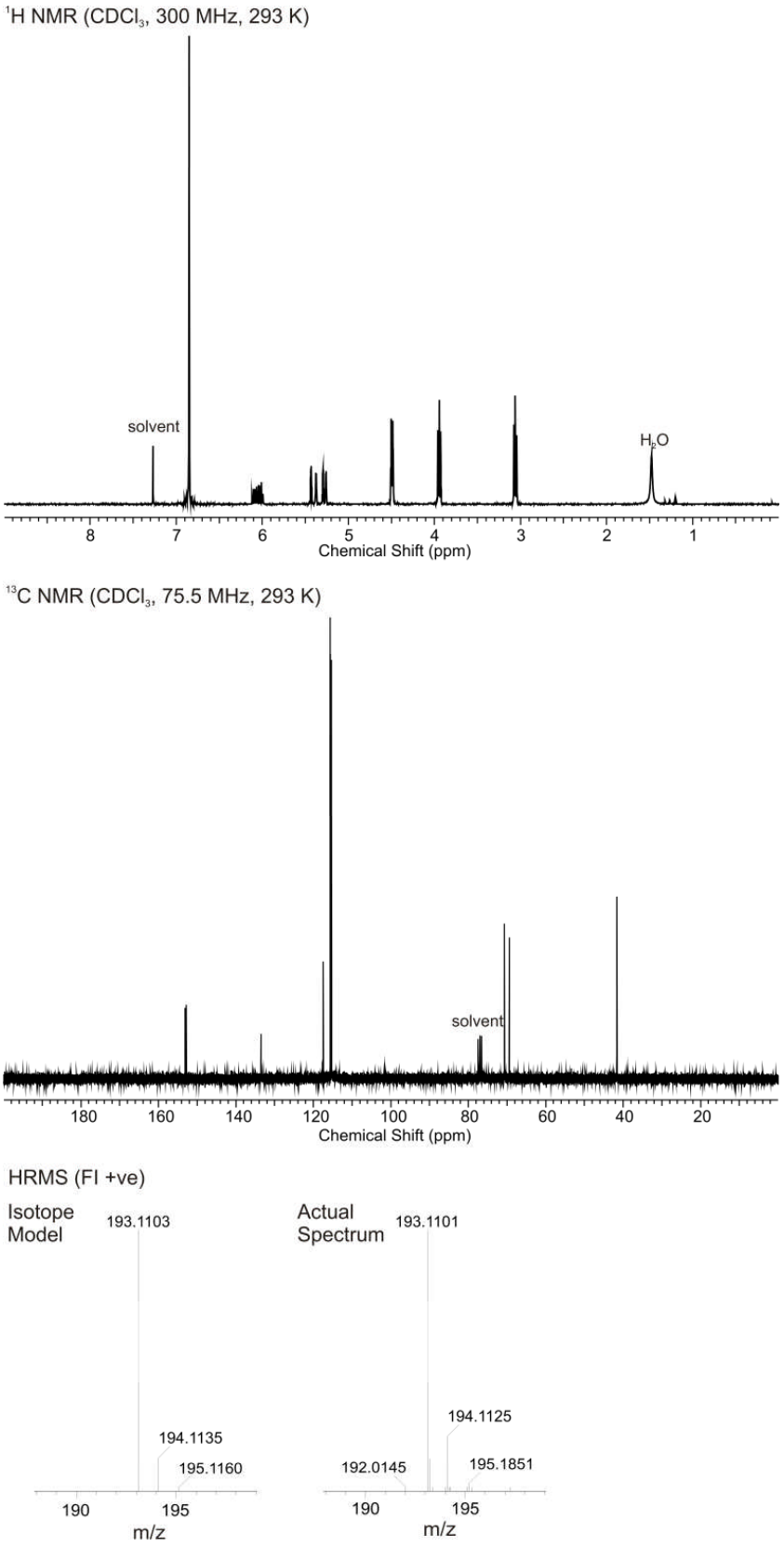

Figure S4: Spectral characterization of compound **6**.

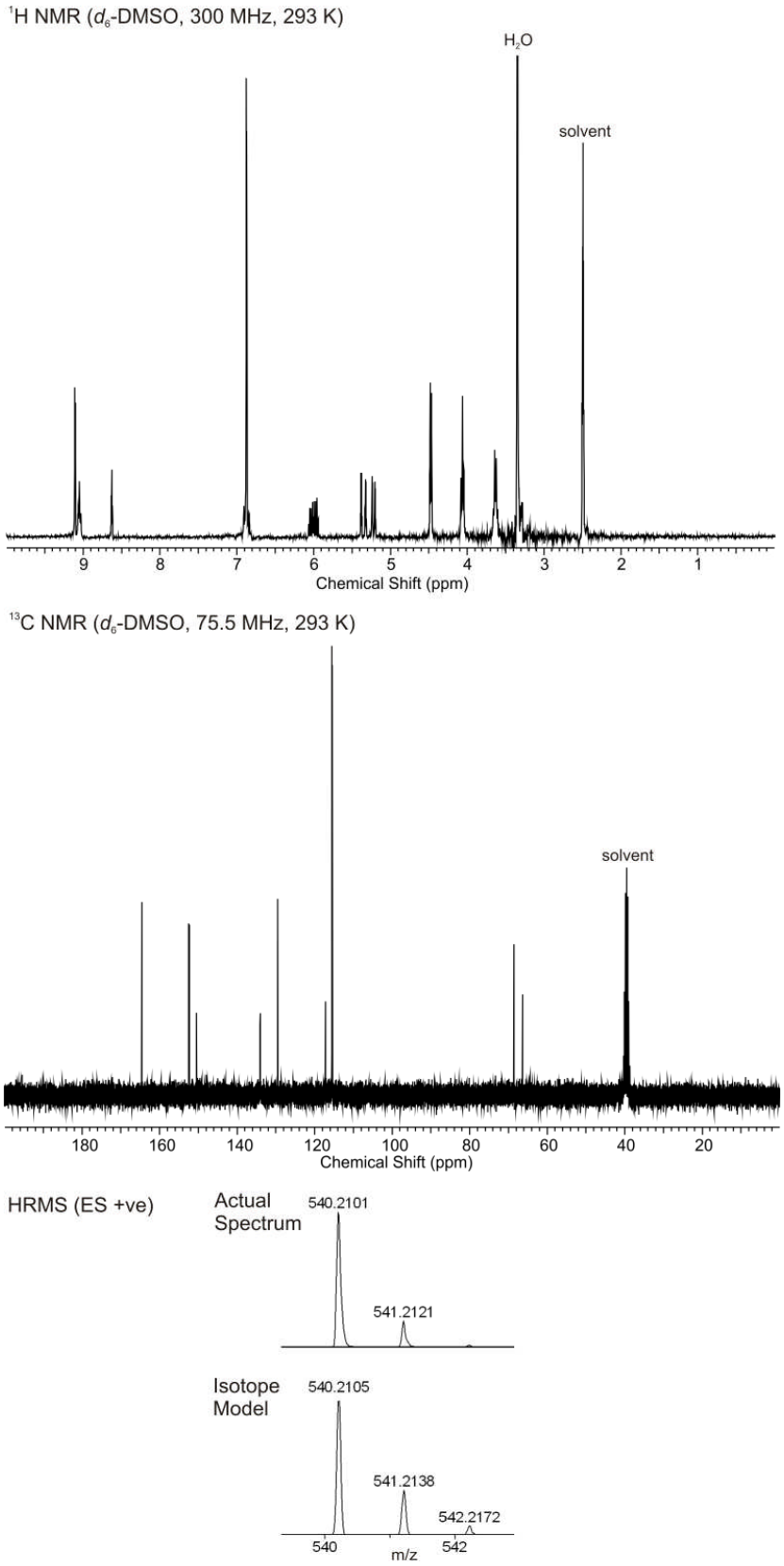

Figure S5: Spectral characterization of compound **9**.

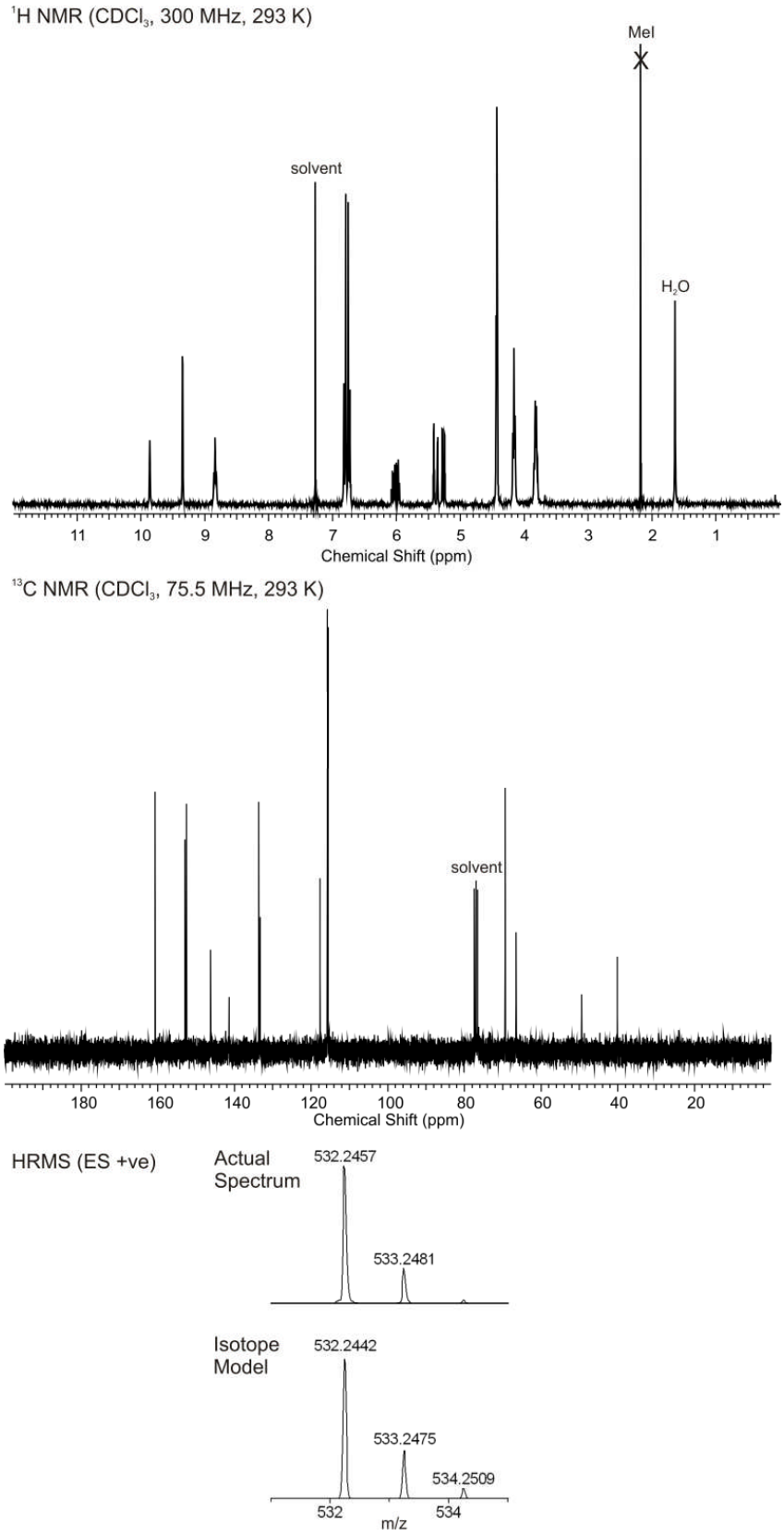

Figure S6: Spectral characterization of compound $\mathbf{3}^{+}(I^{-})$.

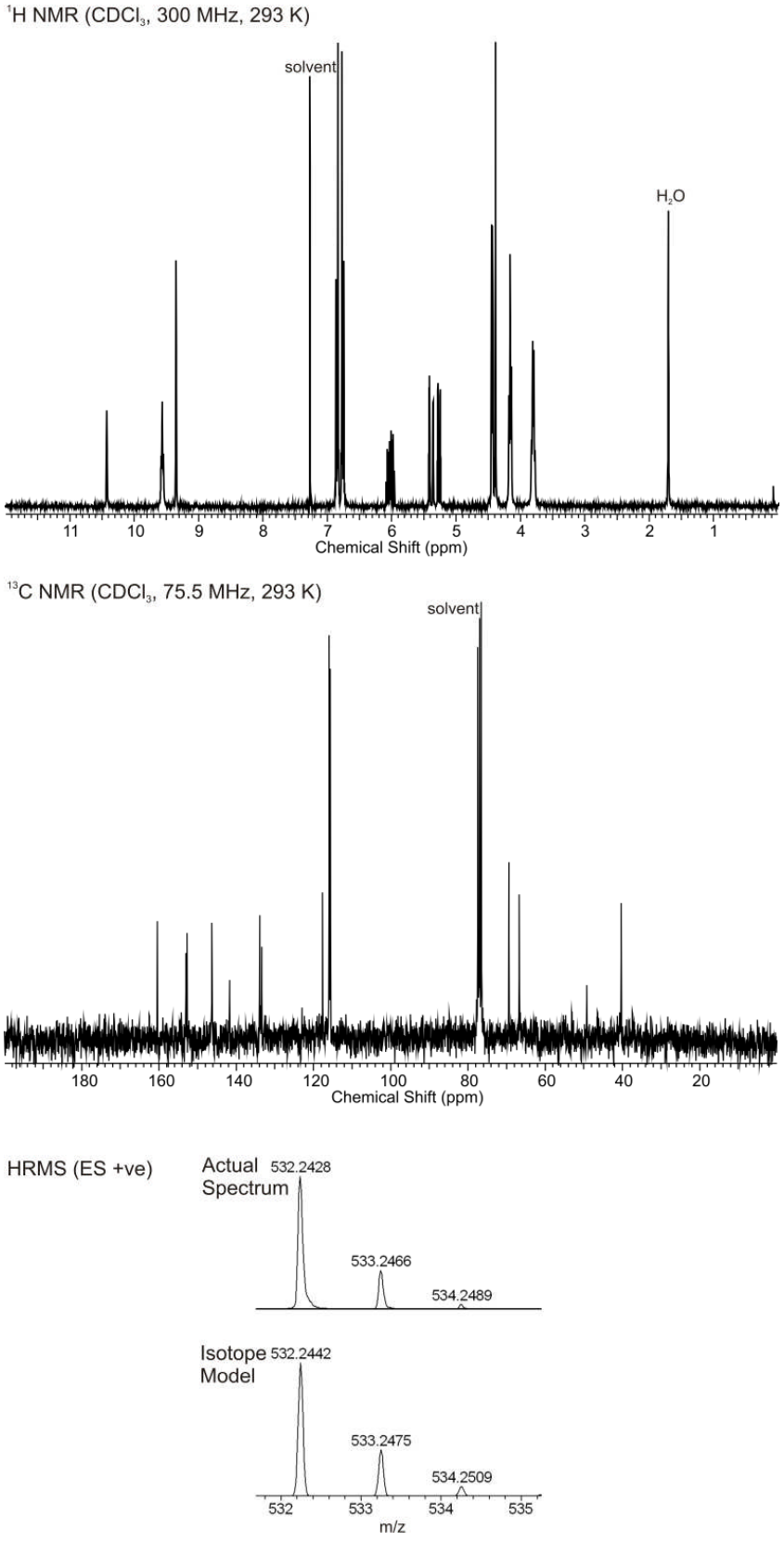

Figure S7: Spectral characterization of compound $\mathbf{3}^{+}(Cl^{-})$.

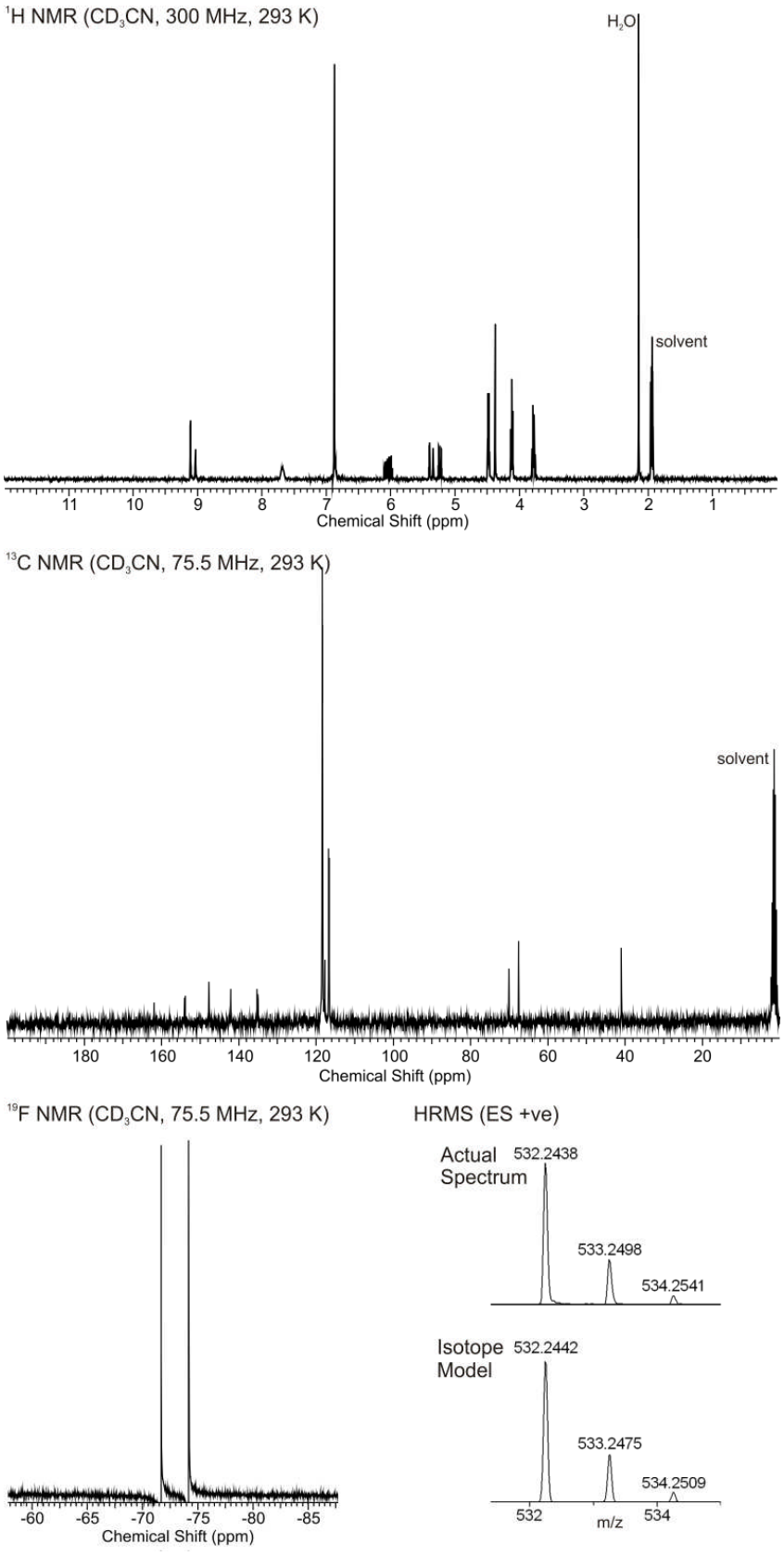

Figure S8: Spectral characterization of compound $\mathbf{3}^{+}(PF_6^{-})$.

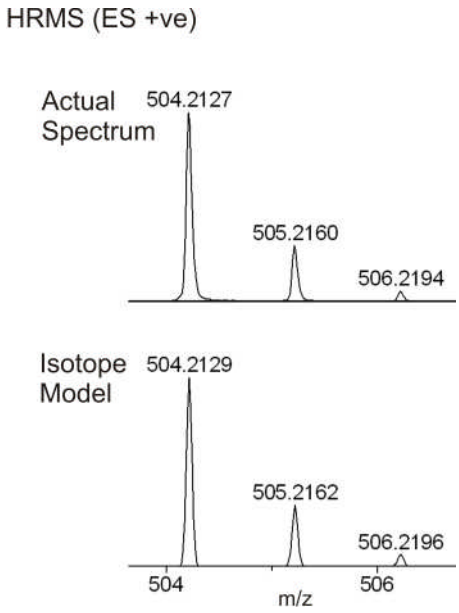

Figure S9: HRMS of compound $\mathbf{13}^{+}(Cl^{-})$.

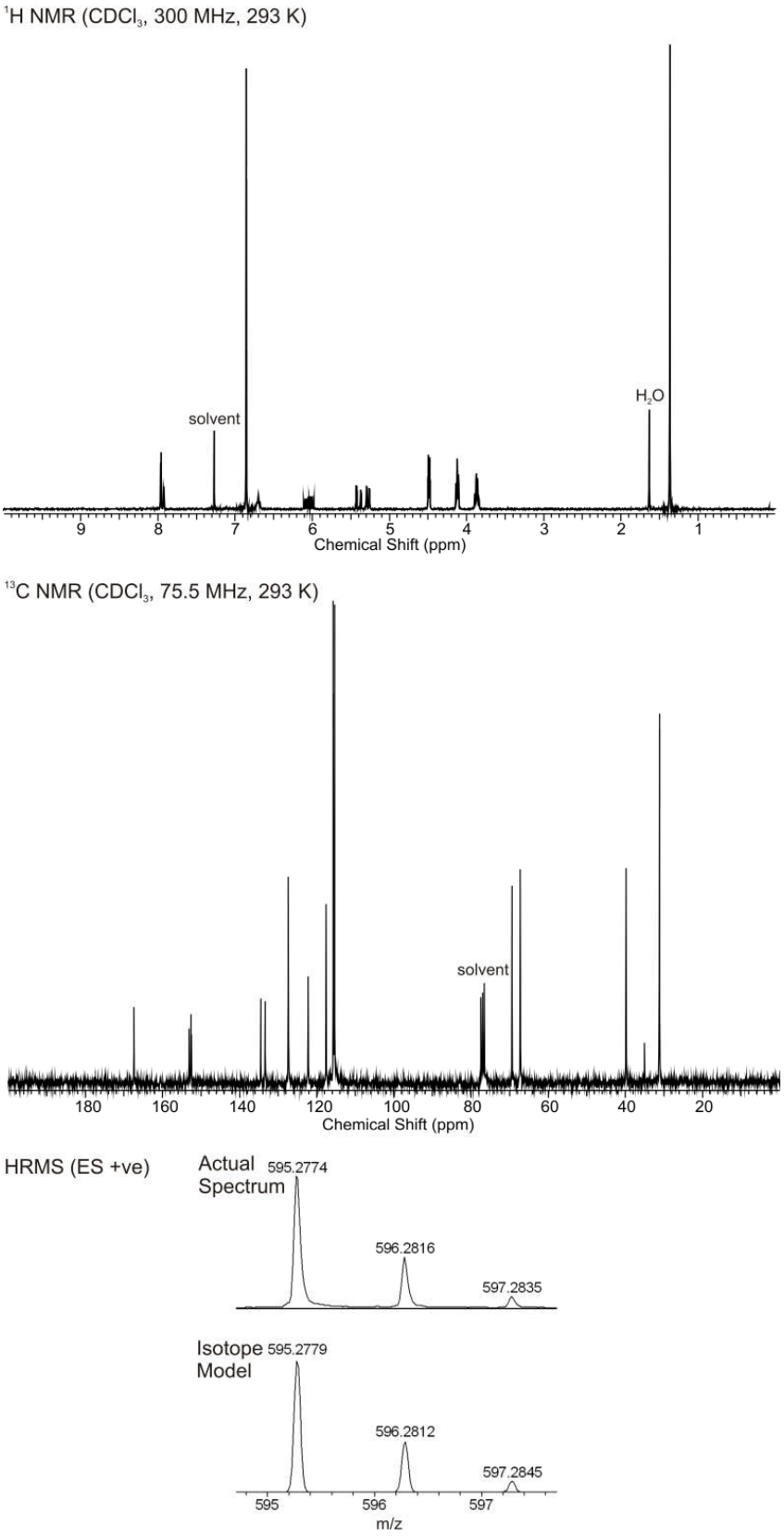

Figure S10: Spectral characterization of compound **S-2**.

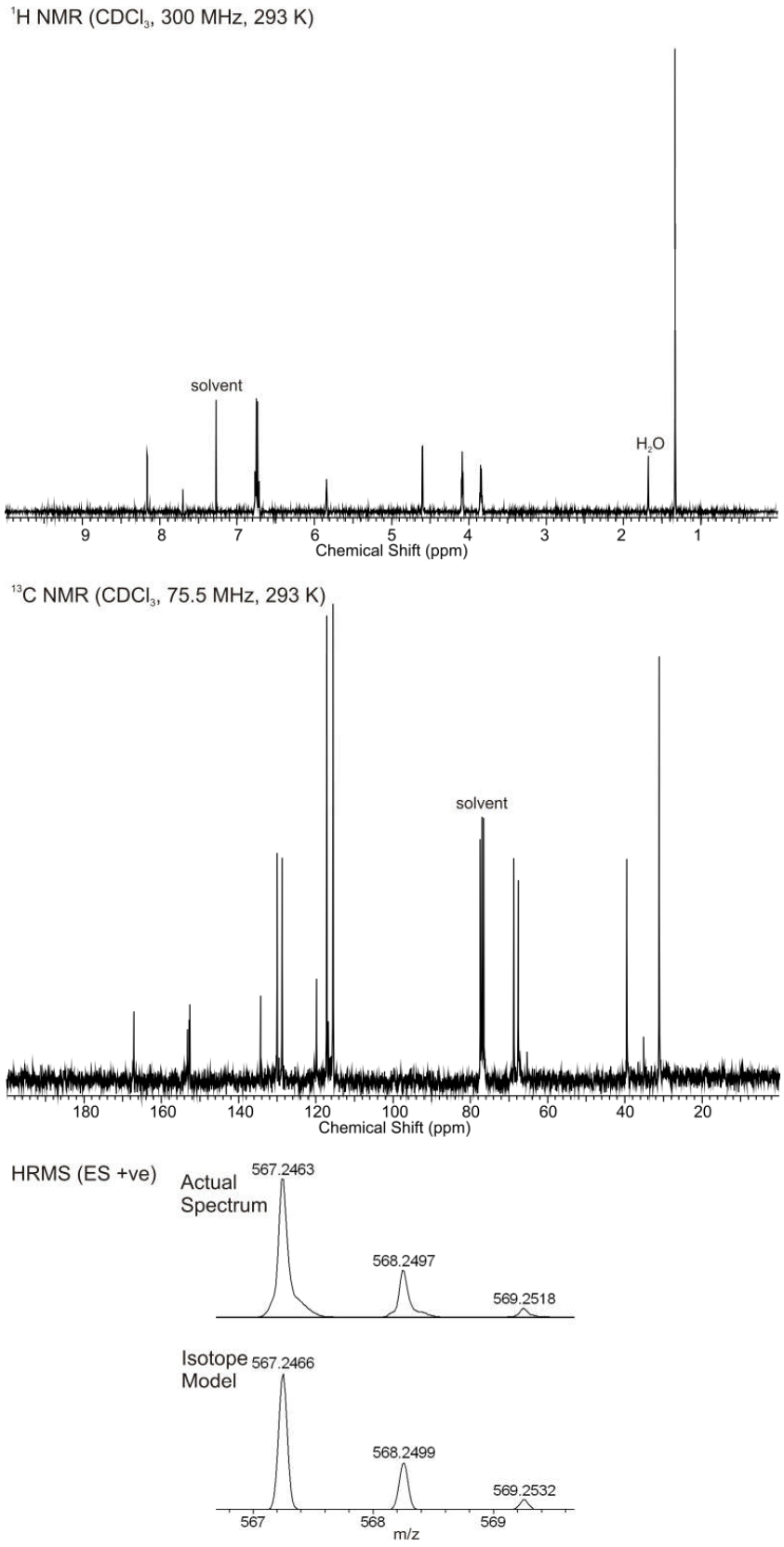

Figure S11: Spectral characterization of compound **14**.

Additional Spectral Comparisons

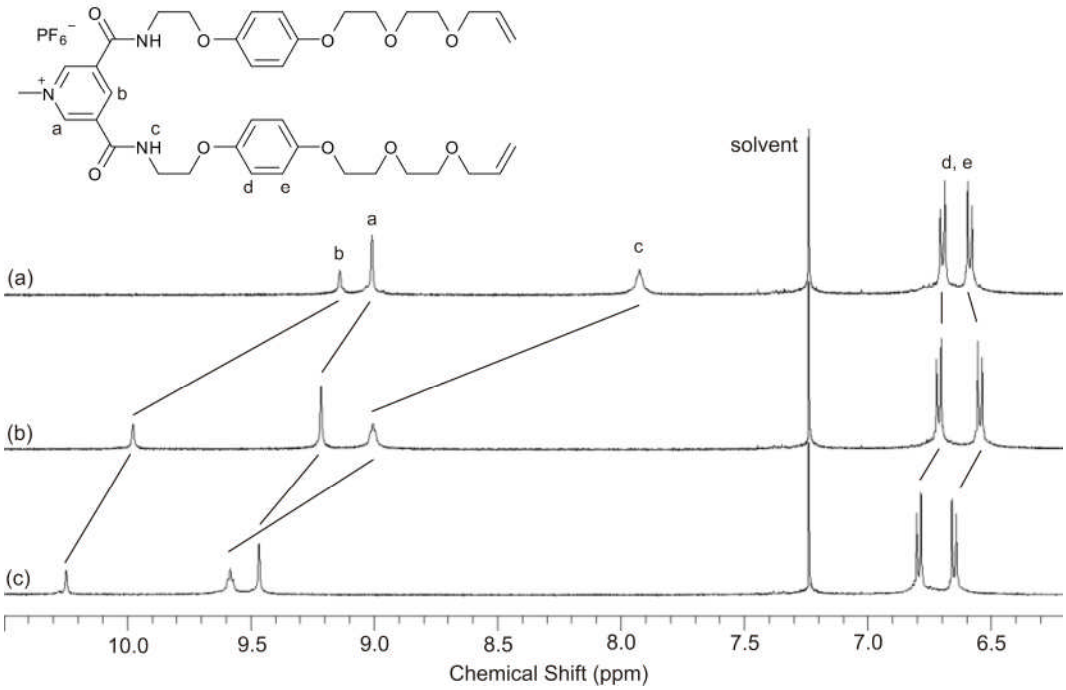

Figure S12: ^{1}H NMR spectra of (a) RCM precursor $\mathbf{1}^{+}(PF_6^{-})$, (b) $\mathbf{1}^{+}(PF_6^{-})$ + 0.5 eq. TBACl and (c) $\mathbf{1}^{+}(PF_6^{-})$ + 1.0 eq. TBACl. Solvent: $CDCl_3$, T = 293 K.

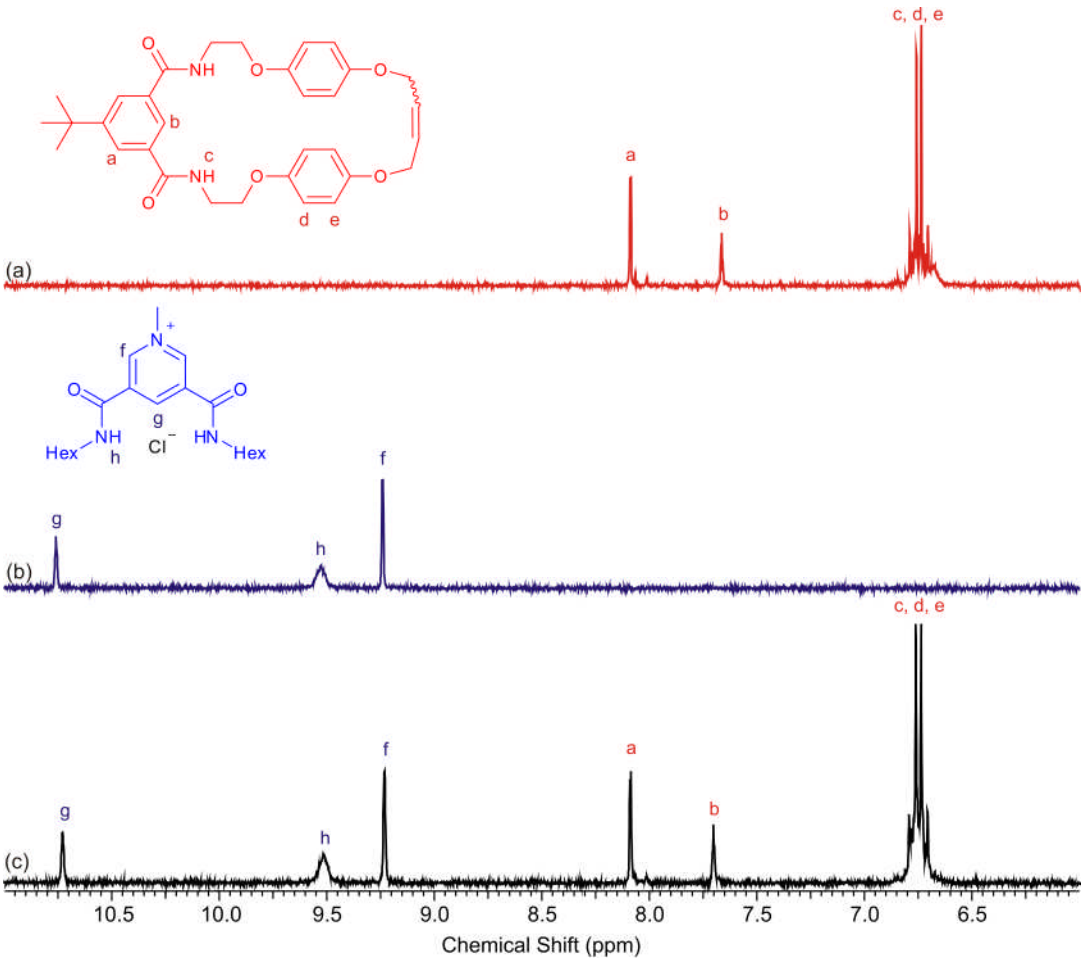

Figure S13: ^{1}H NMR spectra of (a) macrocycle **14**, (b) *N*-methyl pyridinium thread **15**$^{+}$(Cl^{-}) and (c) 1 eq. **14** + 1 eq. **15**$^{+}$(Cl^{-}). Solvent: CD_2Cl_2, T = 293 K.

Crystallography

Crystal Structure of Catenane $\mathbf{11}^{2+}(Cl^-)_2$

Crystals were grown by slow diffusion of di-isopropyl ether into a $CHCl_3/CH_3OH$ solution of catenane $\mathbf{11}^{2+}(Cl^-)_2$. Single crystal X-ray diffraction data were collected using silicon double crystal monochromated synchrotron radiation (λ = 0.68890 Å) at Diamond Light Source beamline I19 using a custom-built Rigaku diffractometer equipped with a Cryostream N_2 open-flow cooling device.[6] The data were collected at 150(2) K via a series of ω-scans were performed in such a way as to cover a sphere of data to a maximum resolution of 0.77 Å. Cell parameters and intensity data (including inter-frame scaling) were processed using the CrystalClear package.[7] The structure was solved by charge flipping using SuperFlip[8] and refined using all data against F^2 within the CRYSTALS suite.[9]

The sample diffracted very weakly, and at high angles the reflections were completely absent, even when subjected to synchrotron radiation. This is ascribed to the large cavity containing disordered solvent. After structure solution, the entire main residue could be modeled but no further structure could be resolved in the solvent cavity, and PLATON SQUEEZE[10] was therefore used to model this diffuse electron density.

Thermal restraints were applied where appropriate to the main residue. Hydrogen atoms were placed geometrically and subsequently constrained using rides. Absent high angle data were omitted from the refinement using the Wilson plot.

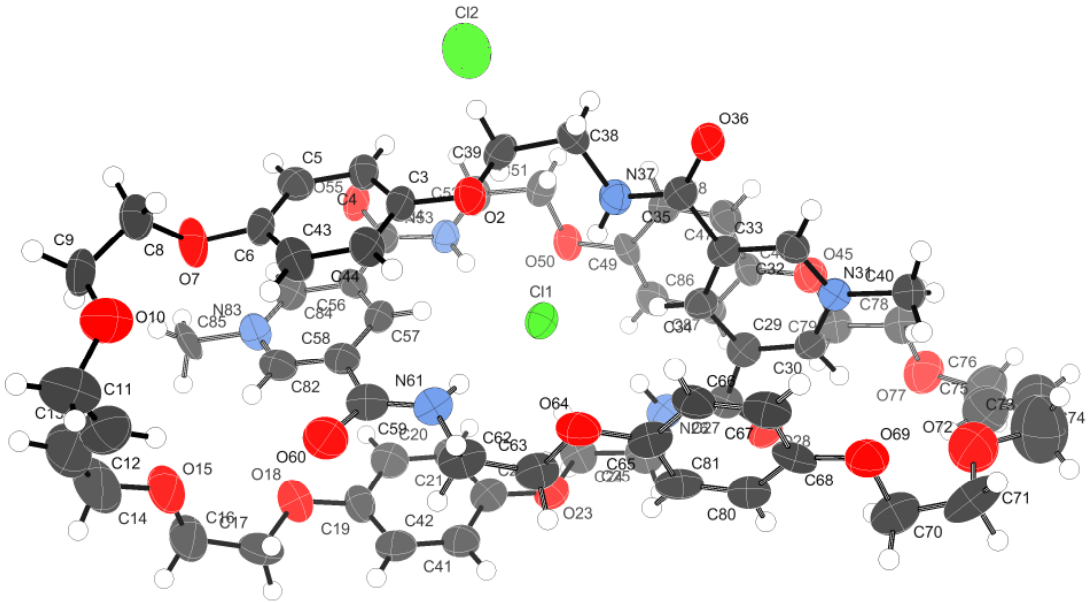

Figure S14: X-ray crystal structure of [2]catenane $\mathbf{11}^{2+}(Cl^-)_2$. Thermal ellipsoids displayed at 50% probability.

Table S1 Selected crystallographic data for [2]catenane $\mathbf{11}^{2+}(Cl^-)_2$

Compound reference	$\mathbf{11}^{2+}(Cl^-)_2$
Chemical formula	$2(C_{32}H_{38}N_3O_8)\bullet_2Cl$
Formula Mass	1256.24
Crystal system	Monoclinic
a/Å	17.303(6)
b/Å	9.051(3)
c/Å	43.048(16)
α/°	90
β/°	95.680(3)
γ/°	90
Unit cell volume/Å^3	6709(4)
Temperature/K	150
Space group	*P*2/*n*
No. of formula units per unit cell, *Z*	4
No. of reflections measured	22082
No. of independent reflections	22082
R_{int}	0.163
Final R_1 values ($I > 2\sigma(I)$)	0.1122
Final $wR(F^2)$ values ($I > 2\sigma(I)$)	0.2568
Final R_1 values (all data)	0.1401
Final $wR(F^2)$ values (all data)	0.2862

Crystal Structure of Catenane $\mathbf{11}^{2+}(Cl^-)(PF_6^-)$

Crystals of $\mathbf{11}^{2+}(Cl^-)(PF_6^-)$ were grown by the slow evaporation of a $CDCl_3/CD_3OD$ solution of $\mathbf{11}^{2+}(PF_6^-)_2$ and excess TBACl. A single crystal having dimensions of approximately 0.24 × 0.36 × 0.58 mm was mounted on a glass fibre using perfluoropolyether oil and cooled rapidly to 150 K in a stream of cold N_2 using an Oxford Cryosystems CRYOSTREAM unit. Diffraction data were measured using an Enraf-Nonius KappaCCD diffractometer (graphite-monochromated MoKα radiation, λ = 0.71073 Å). Intensity data were processed using the DENZO-SMN package.[11]

Examination of the systematic absences of the intensity data showed the space group to be either *P n a* 2_1 or *P n a m*. The structure was solved in the space group *P n a* 2_1 using the direct-methods program SIR92,[12] which located all non-hydrogen atoms. Subsequent full-matrix least-squares refinement was carried out using the CRYSTALS program suite.[9] Coordinates and anisotropic thermal parameters of all non-hydrogen atoms were refined. The NH hydrogen atoms were located in a difference Fourier map and their coordinates and isotropic thermal parameters subsequently refined. Other hydrogen atoms were positioned geometrically after each cycle of refinement. A 3-term Chebychev polynomial weighting scheme was applied. Refinement converged satisfactorily to give *R* = 0.0407, *wR* = 0.0459.

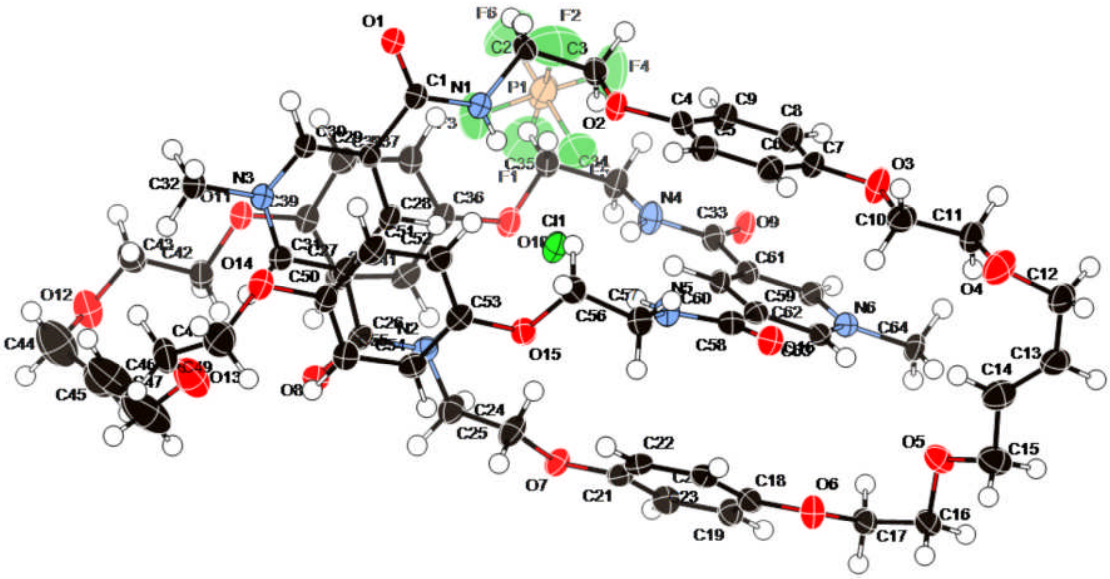

Figure S15: X-ray crystal structure of [2]catenane $\mathbf{11}^{2+}(Cl^-)(PF_6^-)$. Thermal ellipsoids displayed at 50% probability.

Table S2 Selected crystallographic data for [2]catenane $\mathbf{11}^{2+}(Cl^-)(PF_6^-)$.

Compound reference	$\mathbf{11}^{2+}(Cl)(PF_6)$
Chemical formula	$2(C_{32}H_{38}N_3O_8)\bullet ClPF_6$
Formula Mass	1365.75
Crystal system	Orthorhombic
a/Å	30.0276(3)
b/Å	23.8378(3)
c/Å	8.9679(2)
α/°	90
β/°	90
γ/°	90
Unit cell volume/Å^3	6419.15(18)
Temperature/K	150
Space group	*P n a* 2_1
No. of formula units per unit cell, *Z*	4
No. of reflections measured	35133
No. of independent reflections	12903
R_{int}	0.045
Final R_1 values ($I > 2\sigma(I)$)	0.0407
Final $wR(F^2)$ values ($I > 2\sigma(I)$)	0.0459
Final R_1 values (all data)	0.0702
Final $wR(F^2)$ values (all data)	0.0459

Crystal Structure of Catenane $\mathbf{11}^{2+}(SO_4^{2-})$

Crystals were grown by slow diffusion of diisopropyl ether into a dichloromethane/methanol solution of $\mathbf{11}^{2+}(PF_6^-)_2$ and excess TBA_2SO_4. Single crystal X-ray diffraction data were collected using silicon double crystal monochromated synchrotron radiation (λ = 0.68890 Å) at Diamond Light Source beamline I19 using a custom-built Rigaku diffractometer equipped with a Cryostream N_2 open-flow cooling device.[6] The data were collected at 150(2) K via a series of ω-scans were performed in such a way as to cover a half sphere of data to a maximum resolution of 0.77 Å. Cell parameters and intensity data (including inter-frame scaling) were processed using the CrystalClear package.[7]

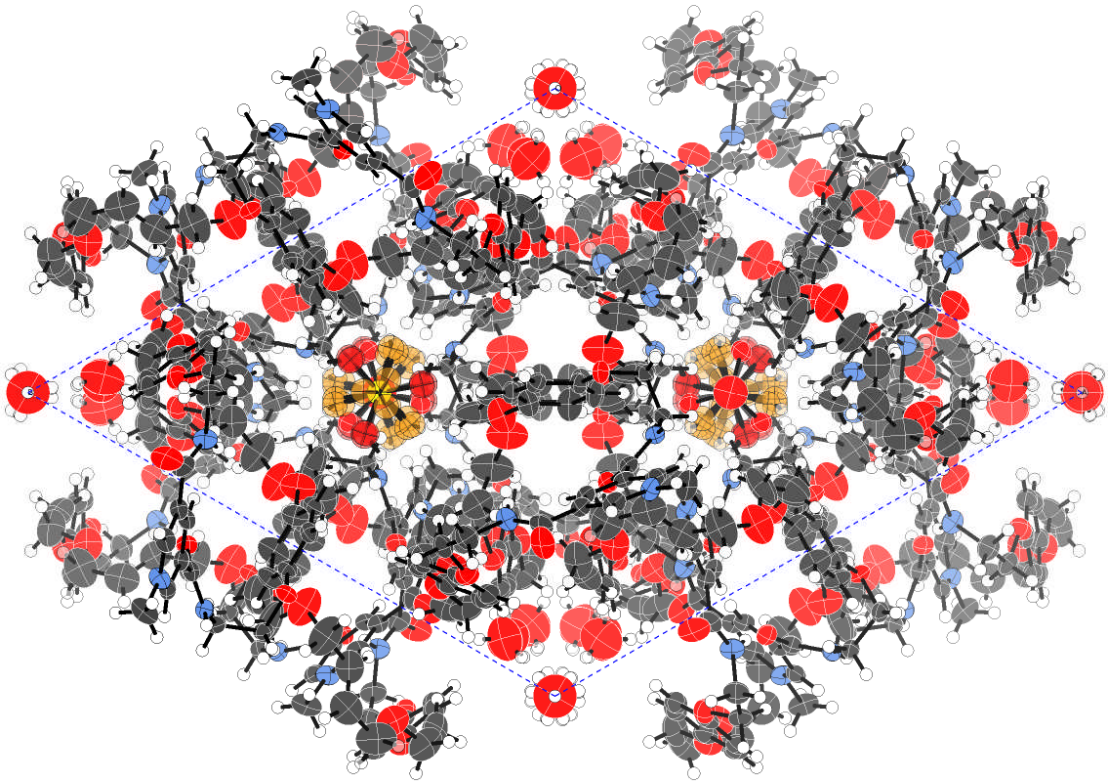

Figure S16: Packing of the [2]catenane mixed sulphate salt showing the 3-fold axes at water (0,0,z) and sulfate (1/3,1/3,z)

The structure could be solved in a variety of space groups, but it was found that P-3c1 (solved using SHELXS 86[12]) yielded a single macrocycle which was related to its catenated partner by symmetry (Figure S16) and gave physically reasonable thermal ellipsoids. Refinement was conducted against all data on F^2 using the CRYSTALS suite.[9] The entire macrocycle and the sulphate anions were obtained from the initial solution, but the co-crystallised water and the hydrogen sulphate anion required iterative cycles of Fourier refinement.

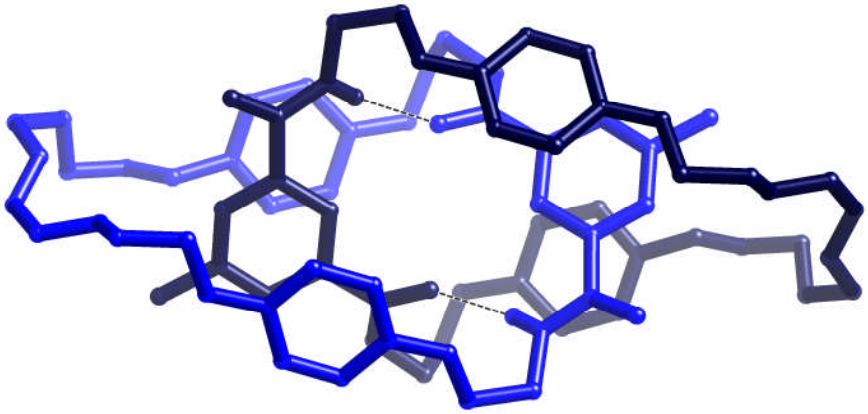

Figure S17: Catenane structure illustrating the inversion-symmetry of the two components and intramolecular amide-amide hydrogen bonding

Due the high level of symmetry in the structure, the precise orientation of hydrogen bonds in the water cluster could not be determined and had to be modelled using partial occupancies. The hydrogen sulfate anion was more complex still. The pseudo-tetrahedron is disordered up/down with respect to the three-fold axis on which it sits (Figure S17). Additionally, one of the components at a slight angle to the axis, producing another level of disorder. Finally, because of the three-fold axis the location of the protonated oxygen (required to balance charge) is also disordered. Restraints were applied to the disordered hydrogensulphate to produce a physically reasonable model, and the hydrogen atom was located to prevent unfavourable charge interactions. This produced a pseudo-cube geometry comprised of the two interpenetrated tetrahedra, consistent with the experimental charge density (Figure S18).

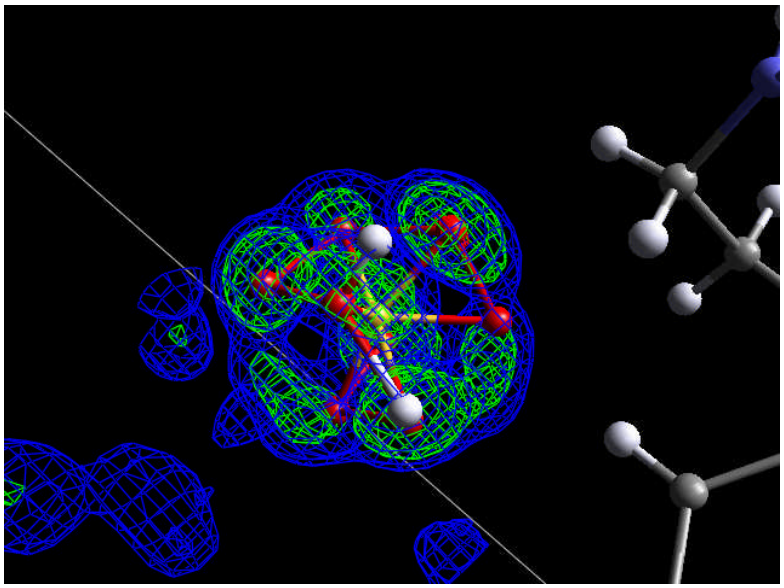

Figure S18: Experimental charge density at the hydrogensulfate anion.

Hydrogen atoms on the main residue were located geometrically and refined against the data using restraints, after which they were constrained using rides.

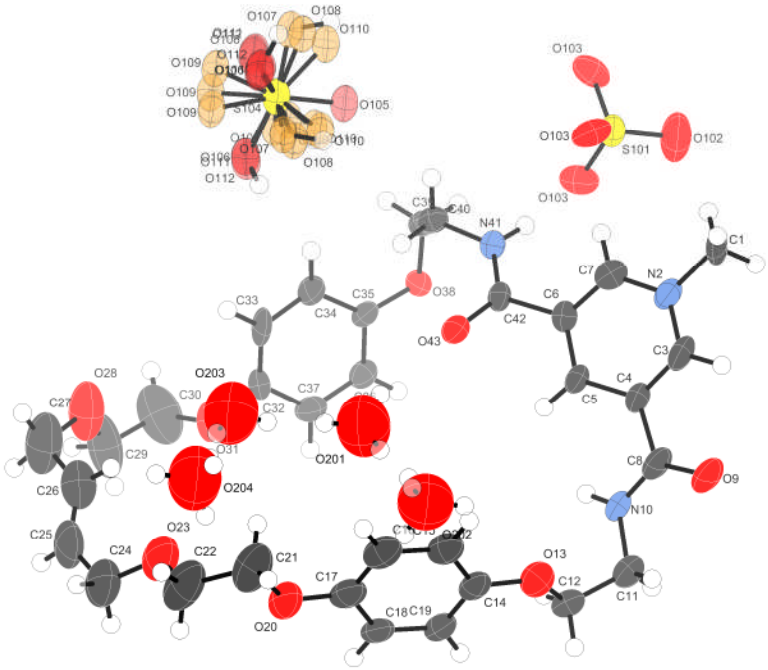

Figure S19: X-ray crystal structure of the mixed sulfate catenane. Thermal ellipsoids displayed at 50% probability. Disordered oxygen atoms in the hydrogensulfate anion shown in red and orange.

Table S3 Selected crystallographic data for [2]catenane $\mathbf{11}^{2+}(SO_4^{2-})$.

Compound reference	$\mathbf{11}^{2+}(SO_4^{2-})$
Chemical formula	$C_{96}H_{131}N_9O_{40}S_2$
Formula Mass	2115.17
Crystal system	Trigonal
a/Å	19.6106(4)
b/Å	19.6106(4)
c/Å	31.5616(8)
α/°	90
β/°	90
γ/°	120
Unit cell volume/Å^3	10511.7(4)
Temperature/K	150
Space group	$P\bar{3}\,c1$
No. of formula units per unit cell, *Z*	4
No. of reflections measured	132460
No. of independent reflections	12709
R_{int}	0.135
Final R_1 values ($I > 2\sigma(I)$)	0.1447
Final $wR(F^2)$ values ($I > 2\sigma(I)$)	0.3511
Final R_1 values (all data)	0.1488
Final $wR(F^2)$ values (all data)	0.3538

^{1}H NMR Titration Protocol

NMR spectra were recorded on a Varian Unity Plus 500 spectrometer. A solution of guest (concentration = 0.0750 moldm^{-3}) was added to a 0.5 mL solution of the host (concentration = 0.0015 moldm^{-3}) at 293 K. The chemical shifts of specific protons of the host were monitored for seventeen titration points (for 0, 0.2, 0.4, 0.6, 0.8, 1.0, 1.2, 1.4, 1.6, 1.8, 2.0, 2.5, 3.0, 4.0, 5.0, 7.0 and 10.0 equivalents of added guest). The resulting data were analysed using the WinEQNMR(2) computer program[13] as the association of guest and host was fast on the NMR timescale.

Anion binding titration experiments were carried out using salts of the non-complexing tetrabutylammonium (TBA) cation as the guest species which were titrated into the host species catenane **11**$^{2+}$(PF_6^-)$_2$ (in 50:50 $CDCl_3$:CD_3OD and 70:30 CD_3CN:D_2O).

The values of the observed chemical shift and the guest concentration were entered for every titration point in the WinEQNMR(2) computer program and estimates for the binding constant, limiting chemical shifts and binding stoichiometry were made. The parameters were refined using non-linear least squares analysis to obtain the best fit between observed and calculated chemical shifts; the program plots the observed shift versus the guest concentration, revealing the accuracy of the experimental data and the suitability of the model used. The input parameters were varied until the best-fit values of the stability constants, together with their errors, converged.

References for Experimental Section

1 K.-Y. Ng, A. R. Cowley and P. D. Beer, *Chem. Commun.*, 2006, 3676-3678.
2 M. R. Sambrook, P. D. Beer, J. A. Wisner, R. L. Paul and A. R. Cowley, *J. Am. Chem. Soc.*, 2004, **126**, 15364-15365.
3 M. D. Lankshear, N. H. Evans, S. R. Bayly and P. D. Beer, *Chem.-Eur. J.*, 2007, **13**, 3861-3870.
4 M. R. Sambrook, P. D. Beer, J. A. Wisner, R. L. Paul, A. R. Cowley, F. Szemes and M. G. B. Drew, *J. Am. Chem Soc.*, 2005, **127**, 2292-2302.
5 A. K. El-Qisairi, H. A. Qaseer and P. M. Henry, *J. Organomet. Chem.*, 2002, **656**, 168-176.
6 J. Cosier and A. M. Glazer, *J. Appl. Cryst.*, 1986, **19**, 105-107.
7 CrystalClear (Version 2.0, 2009), Rigaku Americas, 9009 TX, USA 77381-5209.
8 L. Palatinus and G. Chapuis, *J. Appl. Cryst.*, 1997, **40**, 786-790.
9 P. W. Betteridge, J. R. Carruthers, R. I. Cooper, K. Prout and D. J. Watkin, *J. Appl. Cryst.*, 2003, **36**, 1487.
10 (a) A. Spek, *J. Appl. Cryst.*, 2003, **36**, 7-13; (b) P. van der Sluis and A. L. Spek, *Acta Cryst.*, 1990, **A46**, 194-201.
11 Z. Otwinowski and W. Minor, *Processing of X-ray Diffraction Data Collected in Oscillation Mode*, *Methods Enzymol.* 1997, **276**, Eds C. W. Carter and R. M. Sweet, Academic Press.
12 G. M. Sheldrick, *Acta Cryst.*, 2008, **A64**, 112-122.
13 M. J. Hynes, *J. Chem. Soc., Daltons Trans.*, 1993, 311-312.

Computational Section:

Computational Details

Molecular mechanics calculations (MM) and molecular dynamics (MD) simulations were performed with Amber11.[1] Parameters for $\mathbf{11}^{2+}$ and $\mathbf{10}^{2+}$ with $CH_3CO_2^-$ and $H_2PO_4^-$ were taken from the General AMBER Force Field (GAFF).[2] Their atomic charges were obtained by optimizing the structure (for $\mathbf{11}^{2+}$ and $\mathbf{10}^{2+}$ we optimized its individual component $\mathbf{2}^+$ and $\mathbf{1}^+$) at the HF/6-31G* level of theory using Gaussian03[3] followed by the fitting of the atomic charges to the electrostatic potential (RESP procedure). The $[PF_6]^-$ counter ion was described with parameters and charges taken form the work of Wang *et al*.[4] Methanol and chloroform solvent molecules were described using a full atom model with parameters and charges taken from refs [5] and [6] respectively, while for acetonitrile we used the parameters and charges proposed by Jaime *et al*.[7] Water was described with the standard TIP3P model[8] whereas van der Waals parameters for Cl^- were taken from reference [9] and assigning a -1 partial charge.

As starting geometries for the simulations, the X-ray structure of $\mathbf{11}^{2+}(Cl^-)(PF_6^-)$ and $\mathbf{10}^{2+}(Cl^-)(PF_6^-)$ were used. For $\mathbf{11}^{2+}(X^-)$ and $\mathbf{10}^{2+}(X^-)$ with $X^- = CH_3CO_2^-$, $H_2PO_4^-$, where no X-ray structure was available, a gas-phase quenched dynamics simulation[10] was performed consisting on heating of the models up to 2000 K, followed by a 2 ns collection run, thus generating 20000 conformations. These were minimized by molecular mechanics (MM) through 1000 steps of steepest descent method, followed by the conjugate gradient method until a convergence criterion of 0.0001 kcal mol^{-1} was achieved. The energies were sorted by MM energy and the lowest energy co-conformations were used.

All binding arrangements were solvated in individual cubic boxes of $CHCl_3$:CH_3OH and CH_3CN:H_2O mixtures in the appropriate proportions (50:50 or 70:30, respectively) using PACKMOL[11] (typically *ca*. 50 Å in size after equilibration). For $\mathbf{11}^{2+}(X^-)$ and $\mathbf{10}^{2+}(X^-)$ with $X^- = CH_3CO_2^-$, $H_2PO_4^-$, the $[PF_6]^-$ counter ion was randomly placed around the pyridinium moiety. In all simulations, this counter ion rapidly dissociates, so the initial position of $[PF_6]^-$ does not appear to be important.

The explicit solvent MD simulations started with an initial MM solvent and solute relaxation, followed by 50 ps of NVT heating to 300 K using the Langevin thermostat with a collision frequency of 1 ps^{-1}. The system was then equilibrated for 1 ns in NPT ensemble at 1 atm with isotropic pressure scaling and a relaxation time of 2 ps. The collection of data was performed at 300 K in a NVT ensemble during 25 ns taking advantage of the new AMBER ability to use NVIDIA GPUs[12] to accelerate explicit solvent Particle Mesh Ewald (PME) calculations[13] The SHAKE[14] algorithm was employed in all solution simulations to constrain all bonds involving hydrogens, thus allowing the usage of 2 fs time steps. The non-bonded van der Waals interactions were truncated with a 12 Å cutoff while PME was used to describe the long range electrostatic interactions. The analysis of the trajectories was performed with the PTRAJ utility of AmberTools1.4. The MD trajectories were clustered by RMSd similarity (catenane and anion) using the average-linkage clustering algorithm.[15] The representative co-conformations for all associations were taken as the representative snapshot of the cluster

with larger population. The hydrogen bond analysis between the anions and the catenane binding pocket was monitored considering a N··O/Cl^- distance cutoff of 4 Å and an N-H···O/Cl angle cutoff of 120º. The molecular diagrams were drawn with PyMOL[16] while graphics were plotted with Gnuplot.[17]

Additional Data and Discussion

Tables of the hydrogen bond analyses (% occupancy) performed for ***11***$^{2+}$*(*X^-*),* X^- *=* Cl^-*,* OAc^-*,* $H_2PO_4^-$*.*

Table S4 – Hydrogen bond analysis (% occupancy)[a] performed for **11**$^{2+}$(Cl^-). The acceptors were taken as the four N-H binding sites and the donor is the chloride anion. The N···Cl^- distance cutoff was 4 Å, and the N-H··· Cl^- angle cutoff was 120º.

	N1	N2	N3	N4
Cl^- [$CHCl_3$:CH_3OH; 1:1]	94.02	92.48	92.92	91.81
Cl^- [CH_3CN:H_2O; 70:30]	30.60	31.55	32.02	32.44

[a] % occupancy is the percent of time the hydrogen bond is formed over the trajectory.

Table S5 – Hydrogen bond analysis (% occupancy) performed for **11**$^{2+}$(OAc^-) in $CHCl_3$:CH_3OH (1:1). The acceptors were taken as the four N-H binding sites and the donors are the acetate oxygen atoms. The N···O distance cutoff was 4 Å, and the N-H···O angle cutoff was 120º.

	N1	N2	N3	N4
O1	25.10	87.04	83.64	88.87
O2	80.12	47.60	23.24	21.90

Table S6 – Hydrogen bond analysis (% occupancy) performed for **11**$^{2+}$($H_2PO_4^-$) in $CHCl_3$:CH_3OH (1:1). The acceptors were taken as the four N-H binding sites and the donors are the $H_2PO_4^-$ oxygen atoms. The N···O distance cutoff was 4 Å, and the N-H···O angle cutoff was 120º.

	N1	N2	N3	N4
O	34.09	20.17	70.10	42.34
O	68.57	63.25	38.25	65.26
OH	2.78	33.10	9.81	11.88
OH	10.61	19.37	18.22	6.74

Notes on Modelling of ***10***$^{2+}$*(*X^-*),* X^- *=* Cl^-*,* OAc^-*,* $H_2PO_4^-$ *in 50:50* $CHCl_3$*:*CH_3OH*.*

In order to provide further insights into the anion recognition properties of the catenane **10**$^{2+}$(PF_6^-)$_2$, molecular dynamics (MD) simulations were performed on **10**$^{2+}$(PF_6^-)$_2$ in its association with Cl^-, OAc^- and $H_2PO_4^-$.

Using the X-ray structure of **10**$^{2+}$(Cl^-)(PF_6^-) as a starting geometry, the catenane was immersed in cubic solvent boxes containing a 1:1 chloroform-methanol mixture, with structural data being collected during a 25 ns simulation. For the associations of the oxoanions OAc^- and $H_2PO_4^-$ with the catenane, structures obtained from gas-phase quenched dynamic simulations were used. The experimental details of these simulations

are given below. The representative co-conformations for anion catenane $\mathbf{10}^{2+}$ associations obtained from clustering the MD trajectories are represented in Figure S19.

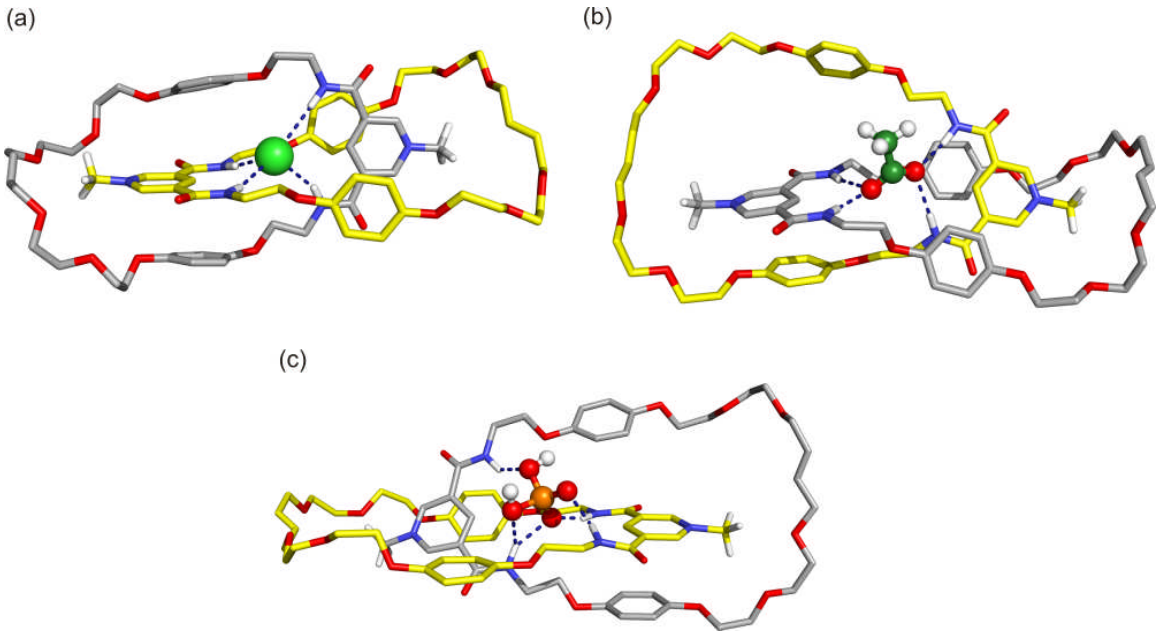

Figure S19: Representative co-conformations of (a) $\mathbf{10}^{2+}(Cl^-)$, (b) $\mathbf{10}^{2+}(OAc^-)$, and (c) $\mathbf{10}^{2+}(H_2PO_4^-)$ in 1:1 chloroform-methanol solution. The solvent molecules and PF_6^- counter ion were omitted for clarity. Relevant hydrogen bonds are represented in dark blue dashed lines. The C-H hydrogen atoms have been omitted apart the *N*-methyl pyridinium ones.

The representative snapshot of catenane $\mathbf{10}^{2+}(Cl^-)$ in solution (Figure 19a) shows the chloride anion residing in the tetrahedral binding cavity (defined by the four amide binding sites), establishing four N-H···Cl hydrogen bonds and presenting a remarkable similarity with the X-ray structure. The *N*-methyl pyridinium rings are sandwiched between the hydroquinone rings of the other macrocycle establishing π-π interactions which are consistent with the experimental structural findings. The replacement of the monoatomic chloride anion by the polyatomic acetate (Figure 19b) results in a distortion of the tetrahedral binding cavity in order to accommodate the carboxylate group of the anion, however this distortion is less than in $\mathbf{11}^{2+}(OAc^-)$, owing to the larger size of $\mathbf{10}^{2+}$. It is also noted in this case, both carboxylate oxygen atoms hydrogen bond simultaneously to two N-H protons of a pyridinium cleft. In $\mathbf{10}^{2+}(H_2PO_4^-)$ the distortion of the tetrahedral arrangement is much less than for $\mathbf{11}^{2+}(H_2PO_4^-)$ (Figure 19c).
The stability of the binding arrangements in this solution mixture were evaluated by monitoring the intermolecular distances between the centre of mass of the binding pocket defined by the four nitrogen atoms of the N-H binding sites (C_{rec}) and Cl^-, or the centre of mass (excluding the hydrogen atoms) of polyatomic anions OAc^- and $H_2PO_4^-$ (C_{anion}), over the duration of the simulation. The evolution of (C_{rec}···C_{anion}) distances during the course of MD simulations is plotted in Figure S20 and the corresponding average distances are given in Table S7.

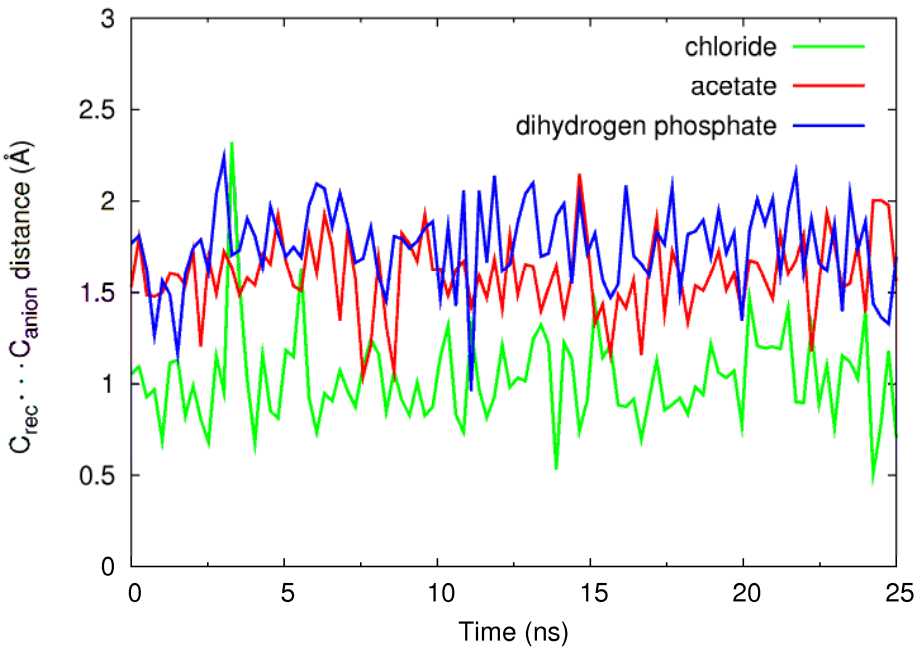

Figure S20: Variations in C_{rec}•••C_{anion} intermolecular distances during the 25 ns of simulation for the binding associations of $\mathbf{10}^{+}$ with Cl^- (green), $H_2PO_4^-$ (blue) and OAc^- (red) anions. The data was smoothed using a cubic spline interpolation.

	Cl^-	$H_2PO_4^-$	OAc^-
$\mathbf{10}^{2+}$	1.04±0.30	1.73±0.25	1.59±0.20

Table S7: C_R•••C_A average intermolecular distances (Å) for the binding associations of Cl^-, OAc^-, $H_2PO_4^-$ with and $\mathbf{10}^{2+}$, obtained from 25 ns of MD simulations. Standard deviations calculated with n = 25000.

As can be seen in Figure S20, the binding associations of $\mathbf{10}^{2+}$ with chloride, acetate and dihydrogen phosphate are stable during the 25 ns of simulation, the anions being kept hydrogen-bonded, having only short periods during which some of these bonds were interrupted.

References for Computational Section

[1] D. A. Case, T. A. Darden, T. E. Cheatham, III, C. L. Simmerling, J. Wang, R. E. Duke, R. Luo, R. C. Walker, W. Zhang, K. M. Merz, B. Roberts, B. Wang, S. Hayik, A. Roitberg, G. Seabra, I. Kolossváry, K. F. Wong, F. Paesani, J. Vanicek, X. Wu, S. R. Brozell, T. Steinbrecher, H. Gohlke, Q. Cai, X. Ye, J. Wang, M.-J. Hsieh, G. Cui, D. R. Roe, D. H. Mathews, M. G. Seetin, C. Sagui, V. Babin, T. Luchko, S. Gusarov, A. Kovalenko and P. A. Kollman, 2010, AMBER 11, University of California, San Francisco.

[2] J. Wang, R. M. Wolf, J. W. Caldwell, P. A. Kollman and D. A. Case, *J. Comput. Chem.*, 2004, **25**, 1157–1174.

[3] M. J. Frisch, G. W. Trucks, H. B. Schlegel, G. E. Scuseria, M. A. Robb, J. R. Cheeseman, J. J. A. Montgomery, T. Vreven, K. N. Kudin, J. C. Burant, J. M. Millam, S. S. Iyengar, J. Tomasi, V. Barone, B. Mennucci, M. Cossi, G. Scalmani, N. Rega, G. A. Petersson, H. Nakatsuji, M. Hada, M. Ehara, K. Toyota, R. Fukuda, J. Hasegawa, M. Ishida, T. Nakajima, Y. Honda, O. Kitao, H. Nakai, M. Klene, X. Li, J. E. Knox, H. P. Hratchian, J. B. Cross, V. Bakken, C. Adamo, J. Jaramillo, R. Gomperts, R. E. Stratmann, O. Yazyev, A. J. Austin, R. Cammi, C. Pomelli, J. W. Ochterski, P. Y. Ayala, K. Morokuma, G. A. Voth, P. Salvador, J. J. Dannenberg, V. G. Zakrzewski, S. Dapprich, A. D. Daniels, M. C. Strain, O. Farkas, D. K. Malick, A. D. Rabuck, K. Raghavachari, J. B. Foresman, J. V. Ortiz, Q. Cui, A. G. Baboul, S. Clifford, J. Cioslowski, B. B. Stefanov, G. Liu, A. Liashenko, P. Piskorz, I. Komaromi, R. L. Martin, D. J. Fox, T. Keith, M. A. Al-Laham, C. Y. Peng, A. Nanayakkara, M. Challacombe, P. M. W. Gill, B. Johnson, W. Chen, M. W. Wong, C. Gonzalez and J. A. Pople, Gaussian, Inc., Wallingford CT, 2004.

[4] Z. Liu, S. Huang and W. Wang, *J. Phys. Chem. B*, 2004, **108**, 12978-12989.

[5] J.W. Caldwell and P. A. Kollman, *J. Phys. Chem.*, 1995, **99**, 6208-6219.

[6] T. Fox, B.E. Thomas IV, M. McCarrick and P.A. Kollman, *J. Phys. Chem.*, 1996, **100**, 10779-10783.

[7] X. Grabuleda, C. Jaime and P. A Kollman, *J. Comp. Chem.*, 2000, **21**, 901-908.

[8] W. L. Jorgensen, J. Chandrasekhar, J. D. Madura, R. W. Impey and M. L. J .Klein, *Chem. Phys.*, 1983, **79**, 926.

[9] I. S. Joung and T. E. Cheatham III, *J. Phys. Chem. B*, 2008, **112**, 9020–9041.

[10] A. Rappe and C. Casewit, "*Molecular Mechanics Across Chemistry*", University Science Books, Sausalito, CA, 1997.

[11] L. Martínez, R. Andrade, E. G. Birgin and J. M. Martínez, *J. Comp. Chem.*, 2009, **30**, 2157-2164.

[12] (a) see http://ambermd.org/gpus/ (accessed in 2011/04/28); (b) D. Xu, M. J. Williamson and R. C.Walker, *Ann. Rep. Comp. Chem.*, 2010, **6**, 2-19.

[13] (a) T. Darden, D. York, L. Pedersen, *J. Chem. Phys.*, 1993, **98**, 10089–10092; (b) U. Essmann, L. Perera, M. L. Berkowitz, T. Darden, H. Lee and L. G. Pedersen, *J. Chem. Phys.*, 1995, **103**, 8577–8593.

[14] J.-P. Ryckaert, G. Ciccotti and H. J. C. Berendsen, *J. Comput. Phys.*, 1977, **23**, 327–341.

[15] J. Shao, S. W. Tanner, N. Thompson and T. E. Cheatham III, *J. Chem. Theory Comput.*, 2007, **3**, 2312–2334.

[16] PyMOL Molecular Graphics System, Version 1.2r2, DeLano Scientific LLC, 2009.

[17] T. Williams and C. Kelley, *Gnuplot 4.4: An Interactive Plotting Program*, 2010. URL: http://www.gnuplot.info